Role for Wnt signaling in retinal neuropil development: analysis via RNAseq and in vivo somatic CRISPR mutagenesis

Sumeet Sarin[1]*, Elizabeth Zuniga-Sanchez[2]*, Yerbol Z Kurmangaliyev[2], Henry Cousins[1], Mili Patel[1], Jeanette Hernandez[2], Kelvin X Zhang[2], Melanie Samuel[1], Marta Morey[2], Joshua R Sanes[1^], S Lawrence Zipursky[2^]

[1]Center for Brain Science and Department of Molecular and Cellular Biology, Harvard University, Cambridge, MA 02130, USA.

[2]Department of Biological Chemistry, HHMI, David Geffen School of Medicine, University of California, Los Angeles, Los Angeles, CA 90095, USA.

* co-first authors

^ co-senior authors

[2^]Lead contact

Correspondence: sanesj@mcb.harvard.edu (J.R.S.), lzipursky@mednet.ucla.edu (S.L.Z.)

Present addresses:

K.X.Z.: Merck Sharp & Dohme Co., Computational Genomics and Informatics, Boston, MA 02210, USA.

M.M.: Departament de Genètica, Facultat de Biologia and Institut de Biomedicina (IBUB) de la Universitat de Barcelona, Barcelona 08028, Spain.

M.S.: Program in Developmental Biology, Baylor College of Medicine, Houston, TX 77030, USA, Department of Neuroscience, Huffington Center on Aging, Baylor College of Medicine, Houston, TX 77030, USA.

SUMMARY

Screens for genes that orchestrate neural circuit formation in mammals have been hindered by practical constraints of germ-line mutagenesis. To overcome these limitations, we combined RNAseq with somatic CRISPR mutagenesis to study synapse development in the mouse retina. Here synapses occur between cellular layers, forming two multilayered neuropils. The outer neuropil, the outer plexiform layer (OPL), contains synapses made by rod and cone photoreceptor axons on rod and cone bipolar dendrites, respectively. We used RNAseq to identify selectively expressed genes encoding cell surface and secreted proteins and CRISPR-Cas9 electroporation with cell-specific promoters to assess their roles in OPL development. Among the genes identified in this

[2^] Lead contact: lzipursky@mednet.ucla.edu

way are Wnt5a and Wnt5b. They are produced by rod bipolars and activate a non-canonical signaling pathway in rods to regulate early OPL patterning. The approach we use here can be applied to other parts of the brain.

INTRODUCTION

Neural circuits in the mammalian brain comprise vast numbers of cell types interlinked by synapses in complex and highly specific ways. Over the past few decades, many genes that regulate neural development have been identified, including key players in steps ranging from neurogenesis to guidance of axons (Kolodkin and Tessier-Lavigne, 2011). In contrast, our understanding of cellular and molecular mechanisms underlying later developmental steps, such as target recognition, formation and maturation of synapses, and formation of laminated neuropil, remains incomplete.

We have chosen to analyze these steps in the outer retina for several reasons. First, it is one of few regions in the mammalian central nervous system in which all neuronal cell types have been identified and their patterns of synaptic connections mapped (Wässle et al., 2009; Sanes and Zipursky, 2010; Dunn and Wong, 2012; Shekhar et al., 2016; Behrens et al., 2016; Franke et al., 2017). Rod and cone photoreceptors populate the outermost layer of the neural retina, the outer nuclear layer (ONL). Their axons terminate in a thin neuropil, the outer plexiform layer (OPL), in which they synapse on interneurons called bipolar and horizontal cells (BCs, HCs), which have somata in an inner nuclear layer (INL) (Figure 1A). Synaptic connectivity within the OPL is stereotyped and highly specific, with rods synapsing predominantly on rod BCs (RBCs) and axons of HCs in the outer sublamina of the OPL, and cones synapsing on cone BCs (CBCs) and HC dendrites in an inner sublamina. Second, the OPL is readily accessible to analysis and manipulation. OPL synapses are large and form postnatally (Olney, 1968; Blanks et al., 1974) and cell type-specific markers are available to monitor pre- and post-synaptic partners in the OPL. Moreover, many types of outer retinal cells can be transduced by electroporation of neonatal retina *in vivo* (Matsuda and Cepko, 2004; 2007). This permits manipulation of the cells that form the OPL before and as it develops. Third, because the synaptic partners are “born” at sites close to their final destinations, and connect by short axons and dendrites, long-distance migration and axon guidance can largely be ignored.

In considering approaches to finding candidate mediators of late steps in circuit assembly, a key problem is that the number of plausible candidate mediators is large, while methods for assessing their roles *in vivo* are low-throughput. Many genes that play important roles in neural circuit development were identified based on their homology to genes initially discovered through unbiased forward genetic screens in flies and worms (Benzer, 1967; Brenner, 1974; Vactor et al., 1993; Colón-Ramos et al., 2007; Wright et al., 2012). In contrast, few unbiased screens have been performed in mice (Merte et al., 2010; Bai et al., 2011; Dwyer et al., 2011; Ha et al., 2015), owing to factors including relatively long generation time and small litter size. Instead, molecular and histological approaches have been used to complement homology-based strategies. For example, identification of proteins based on their ability to stimulate axon outgrowth or synaptic differentiation *in vitro*, has led to the isolation and characterization of factors regulating circuit development *in vivo* (Serafini et al., 1994; Drescher et al., 1995; Scheiffele et al., 2000; Umemori et al., 2004; Christopherson et al., 2005; Linhoff et al., 2009). Alternatively, candidates have been identified on the basis of their spatiotemporal expression during development (Nakamoto et al., 1996; Yamagata et al., 2002). Establishing the function of proteins identified in these ways generally relies on the generation of germ-line knockouts in the mouse. However, as is the case for unbiased screens, this “reverse genetic” approach is limited by the expense of generating, breeding and testing germ-line mutants. Thus, the suspicion persists that many key players are being missed.

Advances in molecular biology over the past several years led us to consider an alternative strategy to study neural circuit assembly. First, RNA sequencing technology (Dong et al., 2016), coupled with methods for cell-type purification (Kay et al., 2012; Siegert et al., 2012), enables a comprehensive approach to identifying genes differentially expressed between specific neuronal cell types at critical times in circuit development. And second, clustered regularly interspaced short palindromic repeat- (CRISPR-) based somatic mutagenesis, using viral methods or electroporation, permits generation of homozygous null mutant neurons in otherwise wild-type animals (Holkers et al., 2014; Wang et al., 2014; Swiech et al., 2015; Heidenreich and Zhang, 2016). Here we combine and extend these methods to develop an approach that facilitates the analysis of retinal development in the mouse.

To apply our RNAseq/CRISPR strategy to the OPL, we first used a panel of cell type-specific markers to characterize OPL development, discovering a hitherto unrecognized early step in its formation. We then obtained transcriptomes from rods, cones, RBCs and CBCs at key developmental times, identified differentially expressed genes encoding cell surface and secreted proteins, and tested candidates using CRISPR-Cas9 somatic mutagenesis. We found that Wnt5a and 5b are selectively expressed by RBCs and play a role in patterning the OPL. We use cell type-specific manipulation to show that they act on rods. Finally, we dissect the signaling pathway in rods, combining further CRISPR-Cas9 somatic mutagenesis, cell culture, and conditional germ-line mutagenesis. Together, our results demonstrate a role for non-canonical Wnt signaling in lamina formation and establish a pipeline that can be applied to other regions of the mouse brain.

RESULTS

Development of the OPL

The OPL contains synapses between photoreceptors (rods and cones) and interneurons (HCs, RBCs and CBCs) (Figure 1A). The cell bodies of these neurons are found in the ONL and INL, respectively. CBCs are further subdivided into 14 types, 6 that are inhibited by light (OFF types) and 8 that are excited by light (ON types); (Greene et al., 2016; Shekhar et al., 2016; Franke et al., 2017). Except where indicated, however, we focus on ON CBCs as a set.

To begin our study, we built on previous work to describe the main cellular events of OPL development (reviewed in Hoon et al., 2014; Zhang et al., 2017). Cones and HCs are born during embryogenesis (E12-E17). Rod development begins late in embryogenesis and peaks soon after birth. The first bipolar cells are born just prior to postnatal day (P)0, with peak numbers generated at P3. All ONL and INL neurons are born prior to P10 (Carter-Dawson and LaVail, 1979; Young, 1985). OPL development occurs postnatally. We divide the postnatal processes into three partially overlapping steps: appearance of the OPL (P0-8) (Figures 1B, S1A), synaptogenesis (P4-13) (Figure 1C), and separation of the rod and cone terminals into discrete sublaminae (P9-21) (Figure 1D). Because retinal differentiation proceeds in a center-to-peripheral wave, times refer to central retina.

Appearance of the OPL. By P0 (Figure S1A), the somata of cones and HCs have segregated, with cones found apically (in the future ONL) and HCs basally (in the future

INL), respectively. However, only a small fraction of the rods and bipolars have formed. The boundary between cell types is incomplete with some mixing of cells between them (discussed further below), and the OPL is not yet present (Figure S1A).

By P2-3 (Figure 1B), cone axons extend into the region of HC somata, and HC processes extend into the region of photoreceptor cell bodies. These neurites are joined by those of recently-born rods, leading to the appearance of discontinuous patches of neuropil at the boundary between the future ONL and INL at P4/5. Over the following few days, gaps between these patches are filled as photoreceptor terminals align and increasing numbers of rods extend axons into the neuropil. HC processes extend laterally along a boundary of developing photoreceptor terminals (Hinds and Hinds, 1979; Schnitzer and Rusoff, 1984; Huckfeldt et al., 2009). In parallel, long thin BC processes attached to the apical and basal surfaces of the epithelium retract, and dendrites of BCs invade the nascent OPL (Figure S1C; Morgan et al., 2006). By P8, the OPL forms a continuous layer of axonal and dendritic processes (Figures 1B, S1C'').

Synaptogenesis. Around P3, cone axons bi- or trifurcate forming multiple contacts with individual HC processes (Figure S1B). Typically, one of these contacts appears bulbous, likely representing an early cone terminal. Previous electron micrographic studies described HC dendrites invaginating into cone pedicles at the sites of synaptic ribbon structures to form monads at P4, with dyads forming soon thereafter and rod-HC monads appearing by P8 (Olney, 1968; Blanks et al., 1974; Rich et al., 1997). Although contact between photoreceptor terminals and dendritic processes occurs as early as P3, the presynaptic cytomatrix protein Bassoon does not appear until P7. Thus, the initial photoreceptor-interneuron contacts may not be molecularly specialized.

As BC dendrites form in the OPL (Figure S1C''), they interact with photoreceptor terminals. Cone pedicles form initial contacts with OFF cone bipolar cells at P6 and with ON cone bipolar cells during subsequent days (Sherry et al., 2003). At P7, we find widespread expression of the pre-synaptic protein Bassoon within the OPL, but only sparse clustering of mGluR6 (Grm6), an ON BC-specific postsynaptic glutamate receptor, apposed to cone terminals (Figures 1C, S1C''). By P13, Bassoon and mGluR6 are clearly visible in rod terminals and RBC dendrites, respectively (Figure 1C).

Sublamination. Initially, synapses formed by rods and cones are intermingled within the OPL (Figure 1D). We used cone arrestin and PSD-95 (a presynaptic marker in rods; Koulen et al., 1998) to label cone and rod terminals, respectively. Near the end of the second postnatal week, rod and cone terminals begin to separate, and RBC dendrites extend further towards the ONL. This gives rise to a continuous band of rod spherules with cone pedicles beneath them. Only a small number of rod terminals remain positioned within the sublayer of cone terminals. The segregation of terminals into distinct rod and cone sublaminae is complete by P21.

Sorting of rod somata: In the course of analyzing OPL development, we were surprised to observe that the nascent OPL formed not at the interface between rod and BCs, but rather within the nascent ONL. Indeed, many rods were observed between the nascent OPL and bipolar neurons (Figure 2A,B). We identified the cells beneath the OPL as rods using two methods: expression of the rod-specific terminal fate marker, rhodopsin (Figure 2A), and their unique chromatin pattern when labeled with a nuclear marker (Figure 2B).

Although the OPL, as defined by contacts between cone and HC processes, segregates cone and HC somata into the ONL and INL, rods are found in both cellular layers during the first postnatal week (Figure 2A). Rods were not dispersed through the INL, but were arranged in rows between bipolar somata (marked by Chx10, which is expressed exclusively by bipolar cells and Muller glia in postnatal animals) and the OPL (Figure 2B). On average, 4 rows of rod somata were present in the INL at P4. Subsequently, three events led to a mature OPL: 1) At P5, HCs extended processes that snaked through the INL-population of rods (Figure 2C); 2) By P6, these processes joined the OPL but a few rows of rods remained on the INL side of the OPL (Figure 2C); and 3) By P9, rods and bipolar cells were completely separated by the OPL (Figure 2A,B) as displaced rods slowly disappeared from the INL.

We presume these rods are migrating back across the OPL to the ONL rather than being eliminated by cell death because the ONL increased in size by an equivalent amount during this time (Figure 2D) and we observed occasional rods within the INL (Figure S6F). It is also possible, however, that some ectopic rods are eliminated by apoptosis, or transformed into another cell type (see *Discussion*).

A summary of OPL development is shown in Figure 2E and 2F.

Transcriptomic analysis of photoreceptor and bipolar neurons

We used RNA sequencing (RNAseq) to identify candidate regulators of interactions between photoreceptor axons and BC dendrites. We chose three time points: P7, just after the OPL forms and synaptogenesis with BCs begins; P13, as synaptogenesis nears completion and sublamination begins; and P30, when the OPL is mature. We purified cone and rod photoreceptors separately by fluorescence activated cell sorting (FACS) using transgene markers: Rho-icre;Ai9 for rods and HRGP (Human Red-Green Protein)-cre;Ai9 for cones. We purified ON BCs, which include ON CBCs plus RBCs using Grm6:GFP (Morgan et al., 2006). As appropriate transgenic lines to separate RBCs from CBCs were not available, we performed RNAseq on cells from Grm6:GFP mice that were fixed and immunostained prior to FACS (see Experimental Procedures), allowing us to purify RBCs (GFP+PKC+) and CBCs (GFP+PKC-) from the same retinas. PKC is not highly expressed at P7, so we profiled rod and cone bipolars separately only at P13.

We generated two biological replicates for each cell type at each time point, obtained 23-129 million reads per sample (Table S1), and determined expression levels of annotated genes (Table S2). Expression profiles for the biological replicates were highly correlated (Figure S2A). The purity of each cell type was determined by assessing the expression of previously identified cell-type specific markers. In all cases, cell-type specific markers of the appropriate type were highly enriched and markers of other retinal cell types were present at low levels (Table S3). Approximately 14,000 genes were expressed in one or more cell types at one or more time points.

Differential gene expression analysis. To uncover cell type-specific patterns of gene expression, we performed a pairwise comparison of transcriptomic profiles at each developmental time (Table S4). As expected, many genes were differentially expressed (Figure 3A). At all three time points, two to three-fold more genes were enriched at least 4x in cones compared to rods. Similarly, two-fold more genes were enriched in CBCs compared to RBCs at P13. Differences between photoreceptors and ON BCs were even more striking, consistent with the greater similarity of cones and rods to each other than to BCs.

We also compared each cell type at different developmental times (Table S4). Gene expression differences across times varied over three orders of magnitude (Figure 3A). Marked differences in gene expression were seen for ON BCs whereas cones were more stable across time. Gene expression changes in rods were intermediate between those in ON BCs and cones. These differences, in part, may reflect relative birth dates; cones are generated prenatally, whereas many rods and BCs are newborn at P7 (Young, 1985). Another possibility, discussed below, is that the differences could reflect cell type diversity within each class.

Transcription factors, channels, receptors, and transporters. Unique sets of transcription factors, channels, receptors, and transporters were differentially expressed among the different cell types (Figure S3). Although a few of these had been described previously (Table S3), the vast majority are novel.

Cell surface and secreted proteins. Interactions between neurons are generally mediated by cell surface and secreted proteins (CSP) so we focused on genes that encode them. First, we evaluated enrichment of cell surface proteins among the differentially expressed (DE) genes by determining the fraction of genes associated with the gene ontology category (GO-term) "plasma membrane" (GO:0005886). In total, 11% of the 13,812 genes expressed in this data set were associated with this category (Table S5). More plasma membrane genes were differentially expressed between rods and cones at P7 and P13, and between RBCs and CBCs at P13 than expected by chance (Fisher's exact test, $p<0.05$). Because no GO term is ideally suited to capture all CSPs, we also performed a stepwise curation to generate a list of 793 CSPs from all DE genes (Figure 3B and STAR methods). This allowed us to identify secreted and plasma membrane proteins not covered by the GO term, as well as retaining (i.e. re-identifying) many genes within the "plasma membrane" category.

To analyze candidate mediators of interactions between photoreceptors and BCs, we focused our analysis on P13. In the comparison between rods and cones, there were 41 CSPs enriched in rods and 156 in cones. The comparison between RBCs and CBCs, revealed that nearly 3-fold more were enriched in CBCs than in RBCs (141 vs. 55; Figure 3C). These proteins include members of several superfamilies including Cadherins, Leucine Rich Repeat (LRR) proteins, and Immunoglobulin (Ig)-superfamily proteins, as

well as the tyrosine phosphatase family of transmembrane receptors (Figure 3D) and both secreted proteins and their receptors. Some members of these families have previously been shown to mediate interactions between neurites during circuit assembly (Kolodkin and Tessier-Lavigne, 2011; de Wit and Ghosh, 2016).

The availability of single cell sequencing data from RBCs (a single type) and the eight ON CBC types allowed us to further explore the discrepancy between the enrichment of DE genes in RBCs and ON CBCs. We compared the expression of genes encoding CSPs identified in our study with single cell profiling data (Figures 3E, S2B; for a broader comparison of methods see Shekhar et al., 2016). This analysis showed that each type of ON CBC expresses on average 70% more differentially expressed CSPs than RBCs. Thus, the increase in the diversity of CSPs we observed in CBCs reflects both the number of different ON CBCs and the increased number of CSPs expressed in each CBC type.

CRISPR-based assay to mutate genes in the outer retina

We next developed a method to assay the function of differentially expressed genes by exploiting the ability of CRISPR-Cas9 to mutate target genes in somatic cells (Swiech et al., 2015). Methods have been developed to introduce genes into neonatal retina, prior to OPL formation, using electroporation and viral vectors (Matsuda and Cepko, 2004; Duan et al., 2014; Wang et al., 2014; Yu et al., 2017). We used electroporation due to the relative ease of constructing vectors, and the shortened latency of expression from plasmids compared to viral vectors. We designed at least two 20bp guide RNAs per gene, using criteria detailed in STAR methods, and used *S. pyogenes* Cas9.

Perturbing gene function in rods. Electroporation of neonatal retina transduces dividing precursor populations efficiently, but postmitotic cells are largely refractory (Matsuda and Cepko, 2004; 2007). Electroporation at P0 therefore transduces precursors to rods, BCs, and Muller glial cells, but neither HCs nor cones. To develop an assay, we first targeted Nrl, a transcription factor that is selectively expressed in rods and represses cone fate (Mears et al., 2001). In Nrl mutant mice, rods are converted into cells that exhibit cone-like features (referred to as “cods”), including expression of the cone opsin, S-opsin (Mears et al., 2001), which is readily assayed by immunostaining.

We compared CRISPR-Cas9 targeted Nrl gene inactivation to shRNA-mediated downregulation and a dominant negative construct (Figure 4A-C). In each case, electroporation was performed at P0 and the efficacy of converting rods to cods was assessed at P21 by staining for S-opsin. Retinas were electroporated with: 1. plasmids encoding shRNAs directed towards Nrl; 2. plasmids containing both Cas9 and an sgRNA directed towards Nrl (see Methods); or 3. a plasmid encoding a dominant negative form of Nrl. In the latter two cases, a second plasmid encoding GFP was co-electroporated to mark the transduced cells.

The CRISPR-Cas9 strategy was most successful. Both of the Nrl sgRNAs tested (termed Nrl^{CRISPR}) led to S-opsin expression in 40-50% of GFP-positive cells in the ONL. By contrast, the penetrance of the phenotypes seen with the Nrl shRNAs and the dominant negative construct was approximately 30% and 10%, respectively (Figure 4C). No GFP-positive cells expressed S-opsin in retinas electroporated with a control plasmid. Because one copy of Nrl is sufficient to repress the cone fate, these data indicate that knockout of both alleles in electroporated cells is highly efficient. We sought to increase the efficacy of the method by electroporating a single plasmid encoding GFP, the sgRNA and Cas9 (Ran et al., 2013). This strategy increased the penetrance (S-opsin positive cells/ GFP-positive cells) to ~90% (Figure 4C). In a time course study, we found expression of S-opsin in GFP-positive cells by P6, the earliest time examined. Thus, homozygous mutagenesis and its consequences can be assayed within 5 days of introducing reagents. Based on these results and those of others (Koike-Yusa et al., 2014; Shalem et al., 2014), we used CRISPR-Cas9 in subsequent studies.

To assess the utility of the CRISPR-Cas9 method to knock out genes regulating wiring in rods, we assessed protein expression, and/or loss-of-function phenotypes in retinas in which sgRNAs targeted *Psd-95, Bassoon, Cadm1, and Elfn1*. PSD-95 and Bassoon are abundant components of rod terminals. In these and other cases described below, we chose sgRNAs to mutate the genes at or near the 5' end of the coding sequence, in order to maximize the chance of generating null alleles. In both $Bassoon^{CRISPR}$ and $Psd\text{-}95^{CRISPR}$, protein expression in a subset of rod terminals was eliminated (Figure S4A). Furthermore, HC and BC sprouting was observed in $Bassoon^{CRISPR}$ (Figure 4G), as previously reported in a germ-line mutant allele (Dick et al., 2003). Elfn1 is a leucine-rich repeat protein expressed on the membranes of rod terminals. In germ-line mutants, glutamate receptors

(mGluR6) fail to cluster on dendrites of RBCs (Cao et al., 2015), and a similar loss was apparent in *Elfn1*^{CRISPR} (Figure 4D). *Cadm1* is an Ig-superfamily cell recognition molecule selectively expressed on rods. In *Cadm1*^{CRISPR} retinas, HC processes sprout as previously described in *Cadm1* germline mutants (Ribic et al., 2014). By contrast to Bassoon mutants, however, RBC or CBC sprouting was not seen in either germ-line or *Cadm1*^{CRISPR} alleles (Figure 4G). *Elfn1*^{CRISPR} retinas also did not display sprouting (Figure S4B). Thus, CRISPR-based mutagenesis effectively knocks down proteins localized to synapses, is effective in generating specific OPL wiring phenotypes and can be used to elicit non-autonomous phenotypes.

Perturbing gene function in bipolar cells. To assess CRISPR-Cas9 mutagenesis in bipolar cells we designed sgRNAs against well-established RBC and CBC markers, *Prkca (PKC)* and *Secretagogin (Scgn)*, respectively (Haverkamp et al., 2000; Puthussery et al., 2010), and used the mGluR6 promoter to selectively express Cas9 in ON BCs. The number of PKC-positive GFP-labeled BCs was reduced by 33% in response to *PKC*^{CRISPR}, and the number or Scgn-positive GFP-labeled BCs was reduced by 59% in response to *Scgn*^{CRISPR} compared to controls (Figures 3E, S4C,D). By contrast, *PKC*^{CRISPR} had no effect on Scgn expression and *Scgn*^{CRISPR} had no effect on PKC expression.

Perturbing gene function in cone-like cells ("cods"). Since cone birth occurs prenatally, these cells are not transduced by electroporation at P0. To assay genes selectively expressed in cones, we simultaneously mutated two genes, an sgRNA targeting Nrl to convert rods into cone-like "cods" (Figure 4B) and a second sgRNA encoded on the same plasmid to target a cone-specific gene. Consistent with results from *Nrl* mutant mice, the position and morphology of *Nrl*^{CRISPR}-generated cods were similar to those of cones (Figure 4B). The "cod" outer segments exhibited a cone-like structure and "cod" cell bodies occupied the outer portion of the ONL, which is characteristic of cones (Figures 4B, S4E). Furthermore, cod axon terminals were similar to those of cones. They were larger than rod terminals, stained by the lectin peanut agglutinin (PNA), and resided within the cone terminal sub-lamina of the OPL (Figures 4B, S4E). In addition, the distribution of Cacna1s, a Calcium channel localized to synapses, was ovoid, as in cones, rather than punctate, as in rods (Figures 4B). Finally, gene expression profiles for cods reported recently by Swaroop and colleagues (Kim et al., 2016) were more similar to cone than rod profiles generated in our study (Figure S4F).

To assess the efficacy of this multiplex strategy, we targeted two genes encoding synaptic proteins expressed in cods, *Psd-95* and *Bassoon* (Figures 4F, S4G). In each case, we compared use of two separate plasmids (one encoding Nrl sgRNA and one encoding the Psd-95 or Bassoon sgRNA) with a single multiplex vector encoding both sgRNAs. In both cases, the sgRNA decreased expression of the targeted protein to undetectable levels in many cods, and the fraction of cods mutated was higher with the multiplex plasmid (58% *Nrl/Psd-95* double KO; 80% *Nrl/Bassoon* double KO) than with the two-plasmids separately (40%, *Nrl/Psd-95*; 27%, *Nrl/Bassoon* double KO, Figures 4F, S4G).

In summary, CRISPR-based electroporation reliably induced homozygous mutations in rods, bipolar cells, and cones (i.e. cods).

CRISPR-based mutagenesis of candidate mediators of OPL development

We used CRISPR-based screening to assess the function of differentially expressed cell surface proteins in rods, cones and bipolars. To identify candidates, we first used stringent criteria for differentially expressed genes at FDR 5% with a minimum fold change cut-off greater than 4. These were then ranked based on statistical significance. Second, from the differentially expressed set, we selected genes encoding cell surface or secreted proteins. Third, among these, we prioritized gene families known to be involved in axon guidance and synapse formation (i.e. shown in Figure 3D).

Retinas were electroporated at P0 and phenotypes were scored at P21. In our pilot screen, knock-outs of eight of 30 genes tested led to detectable outer retinal phenotypes (Table S6).

Three phenotypes were, to our knowledge, novel. In *Gpc-2*^{CRISPR} mutants, inactivating a glypican, rod terminals were enlarged by ~50% on average while other aspects of cell morphology appeared unaffected (Figure 5A). *Wisp1*^{CRISPR} inactivates a secreted protein induced by Wnt signaling and this results in rod terminals being positioned more apically within the OPL (Figure 5B). Thus, these genes may be involved in maturation and positioning of rod terminals, respectively. Simultaneous loss of *Wnt5a/5b* gave rise to a supernumerary OPL (discussed further below).

In the five other cases, CRISPR knockouts led to sprouting of interneuronal processes into the ONL. They were: Bassoon, a component of the presynaptic complex (Dick et al., 2003), present in rods and cones; Syndig1L/Capucin, a paralog of Syndig1, which binds AMPA receptors (Kalashnikova et al., 2010), present in cones; Cadm1, an immunoglobulin superfamily adhesion protein (Ribic et al., 2014), present in rods; Tmem108/Retrolinkin, an endosomal trafficking membrane protein (Fu et al., 2011), present in rods; and Ptprz1, a protein tyrosine phosphatase receptor (Maurel et al., 1994), present in bipolar cells. Interneuronal sprouting has also been observed in germ-line *Cacna1f* (Chang et al., 2006), *Ngl-2* (Soto et al., 2013), *Lkb1* (Samuel et al., 2014) and *PlexA4* (Matsuoka et al., 2012) mutants and in aging mouse and human retina (Samuel et al., 2014). Thus, one possibility is that sprouting is a common response to a variety of perturbations of photoreceptors or interneurons. However, we noted three variants of this phenotype that suggest a higher degree of specificity: (1) in *Bassoon*^{CRISPR} (as well as in *Cacnca1* and *Lkb1*) retinas both HCs and BCs sprouted (Figure 4G); (2) in *Nrl*^{CRISPR} *Syndig1L*^{CRISPR}, *Tmem108*^{CRISPR}, *Cadm1*^{CRISPR}, and *Ptprz1*^{CRISPR} only HC sprouting was seen (Figures 4G, 5C,D, S5); and (3) in *Ptprz1*^{CRISPR} retinas, PSD-95-rich puncta, likely reflecting ectopic rod terminals, were seen within the ONL (Figure 5D).

Wnt5 is required for OPL development

As the Wnt5a/5b phenotype was particularly easy to score and the mechanisms regulating the positioning of the OPL were not known, we combined our RNAseq data and CRISPR-based knock-out strategy to explore it further. We initially chose Wnt5a and Wnt5b for analysis because they were selectively expressed by RBCs (Figures 6A, S5D), unique among 19 Wnt ligands. As both Wnt5a and 5b were reported to interact with the same receptors (Keeble et al., 2006; Lin et al., 2010; Yu et al., 2012), we used the multiplex vector to knockout both simultaneously using two separate sets of sgRNAs. Both pairs of sgRNAs induced a partially duplicated neuropil as did each Wnt5 sgRNA separately (Figure 6B, Table S6). The ectopic OPL was separated from the normal OPL by, on average, ~7 µm. One to three layers of somata were present between the two laminae. We used a panel of antibody markers for rods, cones, amacrine cells and bipolar cells to determine their identity. By these criteria, most, if not all, of the intercalated somata were rods (Figure S6A-C).

We used additional markers to assess the composition of the doubled OPL. Both OPLs

in doubled regions comprised processes of rods, cones, RBCs, CBCs and HCs (Figure 6C). Furthermore, the expression of the rod synaptic protein PSD-95 and the apposition between pre- and post-synaptic markers, as assessed using Bassoon and mGluR6, appeared normal within the ectopic OPL (Figure 6D). This is consistent with the presence of synapses between rod terminals and RBC dendrites within this neuropil. Thus, loss of Wnt5 does not affect subcellular localization of synaptic markers, but rather the placement of synapses themselves.

We also inactivated Dishevelled (Dvl), an intracellular mediator of many Wnt-dependent signaling pathways. There are three mammalian Dvl paralogs, one of which, Dvl1, is expressed at highest levels in all outer retinal cells (Figures 6A, S5D). Removal via CRISPR of *Dvl1* also resulted in an ectopic OPL (Figure 6B), confirming that the ectopic OPL phenotype is due to disruption of the Wnt pathway.

Wnt5 acts through a Ryk-dependent pathway

We next used CRISPR-mediated mutagenesis to analyze the mechanism by which Wnt5a/5b signals. Wnts act through canonical (beta catenin-dependent) and non-canonical (beta catenin-independent) pathways, with all canonical and most non-canonical signaling requiring Dvl. To determine which pathway regulates early OPL formation, we assayed Wnt receptors expressed in rods or BCs (Figure 6A). These included Lrp6 for the canonical pathway and the atypical tyrosine kinase Ryk for the non-canonical pathway, (He et al., 1997; Umbhauer et al., 2000; Yao et al., 2004; Kang et al., 2012). Removal of *Lrp6* did not lead to an ectopic neuropil (Figure 7A). Likewise, no alterations in the OPL were observed following removal of canonical Wnt-enhancers *Rspo2* or *Lgr4* or overexpression of *Dkk1*, an inhibitor of the canonical pathway (Figure S5A). By contrast, removal of *Ryk*, using two different sgRNAs, resulted in an ectopic OPL similar to that observed with *Wnt5a/5b*$^{\text{CRISPR}}$ (Figure 7A). The ectopic OPL generated by *Ryk*^{CRISPR}, like that generated by *Wnt5a/5b*^{CRISPR}, included processes of rods, cones, RBCs, CBCs and HCs (Figure 7B). These results suggest that Wnt5a/5b signal through the Ryk receptor.

We next asked through which co-receptor, Ryk mediates this function. Ryk co-receptors include the Fzd- and Vangl-type receptors (Lu et al., 2004; Kim et al., 2008; Andre et al., 2012). The Vangl-family is not expressed in the developing outer retina (Table S2), but

both Fzd4 and Fzd5 are expressed (Figure 6A). Neither *Fzd4*^{CRISPR} nor *Fzd5*^{CRISPR} induced phenotypes when knocked out individually. Because these two receptors could act redundantly, we generated a multiplex vector to simultaneously mutate both of them. Indeed, knocking out both Fzd4 and Fzd5 receptors, resulted in an ectopic OPL (Figure 7A).

We next sought to assess when Wnt5/Ryk signaling from RBCs to rods is required for OPL development. We observed ectopic nascent OPLs surrounding one or two rows of rod somata in *Wnt5a/Wnt5b*^{CRISPR} and *Ryk*^{CRISPR} as early as P6; P6 is the earliest we can visualize PSD-95 expressing rod terminals (Figure 7C). Cone terminals were present in both neuropils as early as P6 (Figure S6C). Thus, Wnt/Ryk signaling is required for the development rather than the maintenance of the OPL.

Together, these data support a model in which Fzd4 and Fzd5 act in combination with Ryk to regulate OPL development by transducing the Wnt5a/Wnt5b signal via a Dvl-dependent non-canonical signaling pathway.

Rods receive the Wnt5 signal

To determine which cells respond to the Wnt5 signal, we inactivated *Ryk* and *Dvl* in different cell types by expressing Cas9 in a cell-type specific manner. We targeted *Ryk*^{CRISPR} and *Dvl*^{CRISPR} to rods or ON BCs using Rhodopsin and mGluR6 promoters, respectively (see STAR methods). In both cases, rod-restricted expression led to an ectopic neuropil. In contrast, no phenotype was observed in animals in which Ryk or Dvl was knocked out of BCs (Figure 7D). Likewise, mutating Fzd10 (the most abundant cone Fzd) or Dvl1 in cods (*Nrl*^{CRISPR} *Fzd10*^{CRISPR} or *Nrl*^{CRISPR} *Dvl1*^{CRISPR}) led to modest levels of HC sprouting but not to formation of a duplicated OPL (Figure S5B-D).

Thus, the Wnt signal appears to act on rods but not cones. Our results did not, however distinguish between a direct effect of Wnt on rods, or relay mechanisms in which RBC-derived Wnt5 acts on another cell that in turn affects rods. To distinguish between these alternatives, we developed a culture system for photoreceptors. Retinas were dissociated at P3 and cultured for 3 days in defined medium. Rods were identified by immunostaining for Rhodopsin. Rods comprised ~70% of the cells in these cultures, corresponding to their prevalence in whole retina (Jeon et al., 1998). In some experiments, we further enriched

rods by purifying them on immunomagnetic beads coated with antibodies to CD73, a rod-specific marker; rods comprised >90% of cells in these cultures.

In both cases, rods formed short neurites under control conditions, and neurite length approximately doubled when medium was supplemented with Wnt5a or Wnt5b (Figure S7). Application of both Wnt5a and 5b together did not enhance neurite outgrowth beyond that observed for each protein individually, suggesting that they act through the same receptor (Figure 7E,F, S7G). To test whether the observed outgrowth was a general response to the presence of Wnt, we applied Wnt3a, an inducer of the beta-catenin dependent/canonical pathway (Yue et al., 2008). Neurite outgrowth of rod cultures was unaffected by Wnt3a (Figure S7A).

To confirm that Wnt5 was indeed acting through Ryk, we cultured rods that had been electroporated with *Ryk*^{CRISPR} *in vivo*, and stained them with an antibody to Ryk. Among transfected Rhodopsin positive cells, >60% showed partial or complete knockdown of Ryk protein (Figures S7B, S7C), demonstrating the efficacy of *Ryk*^{CRISPR}. Neurites of rods lacking Ryk were non-responsive to Wnt5a or Wnt5b, displaying lengths indistinguishable from control conditions (Figures 7E, S7D).

We also used the culture system to assess effects of Wnt5 on cones. When cultured in isolation (following purification with anti-CD133; see STAR methods), cones survived, but failed to extend processes either in the absence or presence of Wnt5. In unpurified cultures, cones did extend processes (Aït-Ali et al., 2015). Whereas Wnt5 increased neurite length of rods in these cultures, it had no detectable effect on the growth of cone neurites (Figures S7E,F).

These data support a model in which Wnt5a/5b produced by rod bipolars acts directly on rods to pattern the OPL.

Germline mutations phenocopy CRISPR-induced somatic mutations

We obtained conditional *Ryk* germ-line mutants (Hollis et al., 2016) and crossed them to the Rho-icre line described above to generate mice in which *Ryk* was selectively deleted from rods, as constitutive Ryk deleted-mice die shortly after birth (Halford et al., 2000). We observed patches of supernumerary OPL (Figure 7G), similar to those observed in

Ryk^{CRISPR} electroporated patches in both hetereozygous (n=2/4) and null (n=1/2) mutants but not in wild type (n=0/3). These results validate two important aspects of our CRISPR mutagenesis method. First, at least in this case, the phenotype of the CRISPR mutants was concordant with that of "gold standard" germ line mutant. Second, the cellular site of action of a gene (rods for Ryk) inferred from the CRISPR mutant was concordant with that inferred from cre-dependent deletion of a germ-line conditional mutant.

We anticipated that the phenotype observed in the *Ryk* germ-line mutant would be more penetrant than that observed in the CRISPR mutant, but in fact the penetrance was similar. This "patchiness" might reflect a genuine biological phenomenon or incomplete deletion of floxed Ryk from photoreceptors. To distinguish between these alternatives, we analyzed a germ-line constitutive *Dvl1* mutant (Lijam et al., 1997). Three of four mutants displayed a supernumerary OPL akin to our *Dvl1*^{CRISPR} electroporated patches, while two heterozygous animals appeared normal (Figure 7H). The composition of the two OPLs was similar to those observed in the CRISPR-patches, with processes of all synaptic partners intermingled in both and the intercalated cells being rods (Figures 7G,H, data not shown). However, the expressivity remained low; each retina displayed a single duplicated event, ~200 um across on average. The low phenotypic incidence indicates that the positioning of the OPL is tightly regulated with likely redundant mechanisms.

We consider models for how the Wnt pathway regulates OPL patterning in the *Discussion.*

DISCUSSION

Proper wiring underlies mental activities, and miswiring is thought to underlie some psychiatric disorders (Cao et al., 2016). Accordingly, it is essential that we understand the mechanisms by which neurites recognize one another and form an organized neuropil during development. Yet, these are difficult issues to address owing to the diversity of neuronal types and the extraordinary specificity of synaptic connections among them. The recent development of cell-specific markers for purifying cells (Kay et al., 2012), RNA sequencing methods for identifying the genes they express (Siegert et al., 2012), and CRISPR-based somatic mutagenesis to assess their function (Holkers et al., 2014; Wang et al., 2014; Swiech et al., 2015; Heidenreich and Zhang, 2016), prompted us to develop a molecular genetic approach to understanding wiring in the mammalian brain.

We focused on the outer retina for studies reported here, not only because of its accessibility and relative simplicity, but also because photoreceptors exhibit at least three forms of synaptic specificity in the OPL: cellular (rods and cones synapse on RBCs and CBCs, respectively); subcellular (rods synapse on HC axons, and cones on their dendrites); and laminar (rod and cone terminals are confined to outer and inner strata, respectively, within the OPL). Although specificity is not absolute (for example rods make a small number of synapses on cone bipolars [Pang et al., 2010]), the relatively simple structure and largely binary nature of synaptic choices in the OPL make it an attractive region for detailed mechanistic analysis of neuropil assembly.

Using RNA sequencing, we identified many cell surface and secreted proteins selectively expressed by rods, cones, RBCs or CBCs. We then demonstrated that inactivation of gene function in somatic cells via CRISPR provides a robust method for assessing the function of these proteins. Following an initial screen, we focused on Wnt signaling, due to novel phenotypes associated with disrupting this pathway. We demonstrated that Wnt5a/5b from rod bipolars signals to rods via a Ryk/Fzd4/Fzd5/Dvl pathway. When this pathway was perturbed on either the sending or receiving side, OPL formation was perturbed.

Non-canonical Wnt signaling from RBCs to rods regulates OPL development

CRISPR-mediated mutagenesis of Wnt5a and Wnt5b led to segments of duplicated OPL. To pinpoint the signaling pathways and cells through which Wnt5a/5b act, we used our RNAseq data to identify putative Wnt receptors and signal transduction components expressed in the outer retina. We found that Wnts act through a non-canonical pathway using Ryk, Fzd4 and Fzd5 as receptors. Finally, we used cell type-specific promoters driving Cas9 to identify rods as the receiving cells. Together, these results show that Wnt5a/5b produced by RBCs is detected by Ryk/Fzd4/5 co-receptors and Dvl in rods, and functions to organize developing neurites into a single neuropil (Figure 7I).

Although CRISPR-based somatic mutations of five Wnt-related genes (Ryk, Dvl1, Wnt5a, Wnt5b, Wnt5a/5b, Fzd4/5) all led to a similar duplicated OPL, the penetrance of the phenotype was low in all cases. We wondered whether this reflected limited ability to mutate genes –for example generation of hypomorphs or heterozygotes rather than homozygous null cells. To test this idea, we analyzed two germline mutants: a constitutive knockout of Dvl1 and a conditional knockout in which Ryk was removed solely from rods.

Animals of both genetic backgrounds phenocopied their CRISPR counterparts not only qualitatively (duplicated OPL) but also with similarly low penetrance. This low penetrance could be due to several factors, including redundancy, presence of genetic modifiers or genetic compensation. Importantly, it is not due to inherent limitations in somatic CRISPR mutagenesis in this tissue.

Our results add to the many roles that Wnts play in synaptic development in worms, flies and mice (Ahmad-Annuar et al., 2006; Klassen and Shen, 2007; Dickins and Salinas, 2013). Ryk has also been implicated in many other aspects of neural development, including neurogenesis, axon guidance, and target selection (reviewed in Fradkin et al., 2010). In the developing spinal cord, for instance, blocking Ryk function inhibits the outgrowth of corticospinal tract axons (Liu et al., 2005). Wnts also act at multiple stages of retinal development, including cell proliferation, determination, and differentiation (Fujimura, 2016). Thus, Wnts, like other major developmental signals (e.g. Hedgehog, FGF and BMPs), act in multiple contexts.

How does Wnt5a/5b regulate OPL development?

The cellular mechanisms by which disruption of Wnt signaling from RBCs to rods affects OPL development remain unclear. We suggest three alternative models. First, consistent with our in vitro experiments, Wnt5 may act directly upon rod terminals to promote growth towards the OPL. In its absence, rod terminals would fail to extend to the definitive OPL, generating an ectopic layer to which processes of cones, BCs and HCs would be recruited.

Second, consistent with roles of Wnt in presynaptic differentiation and maturation in cerebellum (Hall et al., 2000; Ahmad-Annuar et al., 2006), Wnt signaling could stabilize interactions between rod terminals and their targets. Failure to stably adhere may result in retraction. In this scenario, as in the first, misplaced terminals within the ONL would then nucleate a separate OPL.

A third model is suggested by the previously unappreciated aspect of early retinal development we uncovered in our studies of wild type animals. The conventional view of OPL assembly is that it is preceded by histotypic segregation forming a boundary demarcating the interface between two cell classes, photoreceptors (rods and cones)

within the ONL, and interneurons (BCs and HCs) within the INL. We were surprised to find that at early stages, rod somata are present on both sides of the OPL. That is, the OPL initially forms within the ONL. Although this pattern has not, to our knowledge, been discussed, it is apparent in previously published images (Katoh et al., 2010; Brzezinski et al., 2013). As development proceeds, these misplaced rods disappear by migrating into the ONL, converting to bipolar neurons or dying. The ONL expands as the INL contracts, suggesting that the misplaced neurons migrate into the ONL. In this view, Wnt signaling from underlying RBCs could repel or "push" the ectopic rods into the ONL, consistent with well-documented abilities of Wnts to repel axons (Liu et al., 2005; Keeble et al., 2006) and promote directional translocation of cells (Witze et al., 2008). In the absence of Wnt signaling, the ectopic rods persist and, along with HC axons, nucleate a patch of doubled OPL. It is also possible, however, that Wnts affect the fate of postmitotic cells, which are known to transiently retain the capacity to differentiate into either rods or bipolars (Brzezinski et al., 2010; 2013). One attractive feature of this proposed mechanism is that the number of rows of ectopic rods below the OPL during normal development varies between one and four, the same range of rods separating the duplicated OPLs in Wnt pathway mutants.

Typically, detailed phenotypic analysis including live imaging would allow us to discriminate between these models. But given the penetrance of the phenotype, even in traditional knock outs, it is not currently possible to distinguish between them. Thus, discovery of redundant or compensatory pathways may be required to obtain a satisfying view of the cellular mechanisms by which Wnts act.

Advantages of pathway analysis using somatic CRISPR mutagenesis

Many strategies have been used to elucidate cellular and molecular mechanisms underlying circuit assembly in mammals, but all have limitations. Unbiased loss-of-function mutagenesis screens in mice are expensive and laborious. Cultured neurons are useful for studies of synaptogenesis per se, but few culture systems are available that exhibit synaptic specificity or formation of organized neuropil structures such as laminae. "Knock-out" methods are invaluable for testing candidates identified by expression or bioactivity – but the number of candidates that can be tested in this way is limited. By combining RNAseq and somatic CRISPR mutagenesis, we are able to circumvent some of these limitations. RNAseq enables generation of fairly comprehensive lists of candidate

mediators of intercellular interactions. CRISPR mutagenesis via electroporation as we have done here or viral vectors (Holkers et al., 2014) enables testing a relatively large number of candidates in vivo.

Our studies of Wnt signaling illustrate multiple strengths of somatic CRISPR mutagenesis to study postnatal retinal development. First, once we had demonstrated a phenotype for Wnt5, we were able to analyze its signaling mechanisms rather quickly by identifying signal transduction components expressed in the outer retina and mutating them. We tested a total of eight Wnt receptors and signal transduction components to show that Wnt5 signals through a non-canonical Fzd4/Fzd5/Ryk pathway. Similar tests with germ-line methods would have been considerably slower and substantially more expensive.

Second, somatic methods allow interference in specific cells at specified times in development. For example, germ-line deletion of Ryk leads to lethality, so use of conditional mutants and cell-type specific drivers would have been needed to assess its involvement and demonstrate the cells in which it acts. Similarly, as Wnt signaling acts at both early and late stages of retinal development (Fujimura, 2016), additional steps (e.g., use of ligand-activated cre) would have been necessary to disentangle embryonic and postnatal roles.

Third, the use of multiplex vectors permits mutagenesis of multiple genes simultaneously. For instance, whereas deletion of neither Fzd4 nor Fzd5 alone had a detectable effect, the double mutant exhibited a duplicated OPL. Such redundancy (or compensation) is not uncommon in mammalian systems and, thus, it represents a considerable impediment to genetic analysis. Given the small size of sgRNAs, vectors are available that allow for the simultaneous removal of up to 7 genes by multiplexing (Sakuma et al., 2014).

Finally, although we focus here on early OPL formation, our initial analysis of other genes provides evidence that the method can be used to analyze multiple steps in neural development, and can likely be extended to analysis of neural function in adults.

In conclusion, combining RNAseq to identify candidates with somatic CRISPR mutagenesis to test them provides an effective way to analyze mammalian circuit assembly in vivo. Although we developed and validated our methods in retina, we expect

that they can be applied to many brain regions (see Swiech et al., 2015; Shinmyo et al., 2016; Uezu et al., 2016; Wang et al., 2016). Progress in several other areas, including improved ways to introduce CRISPRs, RNAseq, and microscopy, will further enhance the power of this approach, extending the range of problems and regions to which it can be applied.

Acknowledgements

We would like to thank X. William Yang for assistance with our mouse colony and discussions; Xian-Jie Yang, Nick Brecha, Yimin Zou, and Anthony Wynshaw-Boris for generously providing reagents and mouse lines; Donghui Chen and Owen Witte for technical support in cell sorting; and Dorian Gunning for help with the mGluR6 antibody production. We are particularly grateful for advice, mouse lines, and communication of results prior to publication at early stages of our work from Felice Dunn and Rachel Wong. We thank the Sanes and Zipursky labs for comments on the manuscript.

This work was supported by the National Institute of Neurological Disorders and Stroke (T32NS048004*)* and the National Eye Institute (1K99EY028200) to E.Z., Helen Hay Whitney Foundation (E.Z.), Damon Runyon Fellowship (S.S.), and NIH R21 EY025421 (J.R.S.). Gerald Oppenheimer Family Foundation Center for Prevention of Eye Disease Award and Broad Stem Cell Research Center Innovation Award to M.M and S.L.Z. S.L.Z. is an Investigator of the Howard Hughes Medical Institute.

Author Contributions

S.S., E.Z., J.R.S., and S.L.Z. outlined the project and wrote the manuscript. S.S. and E.Z. performed the *in vivo* experiments and analyzed the data. E.Z. carried out the RNA sequencing, and Y.Z.K. and K.X.Z. analyzed the RNA sequencing data. H.C. performed the *in vitro* experiments, M.P. generated the multiplex vectors, J.H. helped carry out the CRISPR screen, and M.S. developed the protocol for sorting and sequencing fixed cells. M.M. initiated this project in the Zipursky lab and carried out the initial RNA sequencing studies.

Declaration of Inerests

The authors declare no competing interests.

References

Ahmad-Annuar, A., Ciani, L., Simeonidis, I., Herreros, J., Fredj, N.B., Rosso, S.B., Hall, A., Brickley, S., and Salinas, P.C. (2006). Signaling across the synapse: a role for Wnt and Dishevelled in presynaptic assembly and neurotransmitter release. J. Cell Biol. *174*, 127–139.

Aït-Ali, N., Fridlich, R., Millet-Puel, G., Clérin, E., Delalande, F., Jaillard, C., Blond, F., Perrocheau, L., Reichman, S., Byrne, L.C., et al. (2015). Rod-derived cone viability factor promotes cone survival by stimulating aerobic glycolysis. Cell *161*, 817–832.

Andre, P., Wang, Q., Wang, N., Gao, B., Schilit, A., Halford, M.M., Stacker, S.A., Zhang, X., and Yang, Y. (2012). The Wnt coreceptor Ryk regulates Wnt/planar cell polarity by modulating the degradation of the core planar cell polarity component Vangl2. J. Biol. Chem. *287*, 44518–44525.

Ashburner, M., Ball, C.A., Blake, J.A., Botstein, D., Butler, H., Cherry, J.M., Davis, A.P., Dolinski, K., Dwight, S.S., Eppig, J.T., et al. (2000). Gene ontology: tool for the unification of biology. The Gene Ontology Consortium. Nat. Genet. *25*, 25–29.

Bai, G., Chivatakarn, O., Bonanomi, D., Lettieri, K., Franco, L., Xia, C., Stein, E., Ma, L., Lewcock, J.W., and Pfaff, S.L. (2011). Presenilin-dependent receptor processing is required for axon guidance. Cell *144*, 106–118.

Behrens, C., Schubert, T., Haverkamp, S., Euler, T., and Berens, P. (2016). Connectivity map of bipolar cells and photoreceptors in the mouse retina. Elife *5*, 1206.

Benzer, S. (1967). BEHAVIORAL MUTANTS OF Drosophila ISOLATED BY COUNTERCURRENT DISTRIBUTION. Proc. Natl. Acad. Sci. U.S.a. *58*, 1112–1119.

Blanks, J.C., Adinolfi, A.M., and Lolley, R.N. (1974). Synaptogenesis in the photoreceptor terminal of the mouse retina. The Journal of Comparative Neurology *156*, 81–93.

Brenner, S. (1974). The genetics of Caenorhabditis elegans. Genetics *77*, 71–94.

Brzezinski, J.A., Lamba, D.A., and Reh, T.A. (2010). Blimp1 controls photoreceptor versus bipolar cell fate choice during retinal development. Development *137*, 619–629.

Brzezinski, J.A., Uoon Park, K., and Reh, T.A. (2013). Blimp1 (Prdm1) prevents re-specification of photoreceptors into retinal bipolar cells by restricting competence. Dev. Biol. *384*, 194–204.

Cao, M., Huang, H., Peng, Y., Dong, Q., and He, Y. (2016). Toward Developmental Connectomics of the Human Brain. Front Neuroanat. *10*, 25.

Cao, Y., Sarria, I., Fehlhaber, K.E., Kamasawa, N., Orlandi, C., James, K.N., Hazen,

J.L., Gardner, M.R., Farzan, M., Lee, A., et al. (2015). Mechanism for Selective Synaptic Wiring of Rod Photoreceptors into the Retinal Circuitry and Its Role in Vision. Neuron *87*, 1248–1260.

Carter-Dawson, L.D., and LaVail, M.M. (1979). Rods and cones in the mouse retina. II. Autoradiographic analysis of cell generation using tritiated thymidine. The Journal of Comparative Neurology *188*, 263–272.

Chang, B., Heckenlively, J.R., Bayley, P.R., Brecha, N.C., Davisson, M.T., Hawes, N.L., Hirano, A.A., Hurd, R.E., Ikeda, A., Johnson, B.A., et al. (2006). The nob2 mouse, a null mutation in Cacna1f: anatomical and functional abnormalities in the outer retina and their consequences on ganglion cell visual responses. Vis. Neurosci. *23*, 11–24.

Chen, Y., Lun, A.T.L., and Smyth, G.K. (2016). From reads to genes to pathways: differential expression analysis of RNA-Seq experiments using Rsubread and the edgeR quasi-likelihood pipeline. F1000Res *5*, 1438.

Christopherson, K.S., Ullian, E.M., Stokes, C.C.A., Mullowney, C.E., Hell, J.W., Agah, A., Lawler, J., Mosher, D.F., Bornstein, P., and Barres, B.A. (2005). Thrombospondins are astrocyte-secreted proteins that promote CNS synaptogenesis. Cell *120*, 421–433.

Colón-Ramos, D.A., Margeta, M.A., and Shen, K. (2007). Glia promote local synaptogenesis through UNC-6 (netrin) signaling in C. elegans. Science *318*, 103–106.

Cong, L., Ran, F.A., Cox, D., Lin, S., Barretto, R., Habib, N., Hsu, P.D., Wu, X., Jiang, W., Marraffini, L.A., et al. (2013). Multiplex genome engineering using CRISPR/Cas systems. Science *339*, 819–823.

de Wit, J., and Ghosh, A. (2016). Specification of synaptic connectivity by cell surface interactions. Nat. Rev. Neurosci. *17*, 22–35.

Dick, O., tom Dieck, S., Altrock, W.D., Ammermüller, J., Weiler, R., Garner, C.C., Gundelfinger, E.D., and Brandstätter, J.H. (2003). The presynaptic active zone protein bassoon is essential for photoreceptor ribbon synapse formation in the retina. Neuron *37*, 775–786.

Dickins, E.M., and Salinas, P.C. (2013). Wnts in action: from synapse formation to synaptic maintenance. Front Cell Neurosci *7*, 162.

Dobin, A., Davis, C.A., Schlesinger, F., Drenkow, J., Zaleski, C., Jha, S., Batut, P., Chaisson, M., and Gingeras, T.R. (2013). STAR: ultrafast universal RNA-seq aligner. Bioinformatics *29*, 15–21.

Dong, X., You, Y., and Wu, J.Q. (2016). Building an RNA Sequencing Transcriptome of the Central Nervous System. Neuroscientist *22*, 579–592.

Drescher, U., Kremoser, C., Handwerker, C., Löschinger, J., Noda, M., and Bonhoeffer, F. (1995). In vitro guidance of retinal ganglion cell axons by RAGS, a 25 kDa tectal protein related to ligands for Eph receptor tyrosine kinases. Cell *82*, 359–370.

Duan, X., Krishnaswamy, A., la Huerta, De, I., and Sanes, J.R. (2014). Type II cadherins

guide assembly of a direction-selective retinal circuit. Cell *158*, 793–807.

Dunn, F.A., and Wong, R.O.L. (2012). Diverse strategies engaged in establishing stereotypic wiring patterns among neurons sharing a common input at the visual system's first synapse. J. Neurosci. *32*, 10306–10317.

Dwyer, N.D., Manning, D.K., Moran, J.L., Mudbhary, R., Fleming, M.S., Favero, C.B., Vock, V.M., O'Leary, D.D.M., Walsh, C.A., and Beier, D.R. (2011). A forward genetic screen with a thalamocortical axon reporter mouse yields novel neurodevelopment mutants and a distinct emx2 mutant phenotype. Neural Dev *6*, 3.

Fradkin, L.G., Dura, J.-M., and Noordermeer, J.N. (2010). Ryks: new partners for Wnts in the developing and regenerating nervous system. Trends Neurosci. *33*, 84–92.

Franke, K., Berens, P., Schubert, T., Bethge, M., Euler, T., and Baden, T. (2017). Inhibition decorrelates visual feature representations in the inner retina. Nature *542*, 439–444.

Fu, X., Yang, Y., Xu, C., Niu, Y., Chen, T., Zhou, Q., and Liu, J.-J. (2011). Retrolinkin cooperates with endophilin A1 to mediate BDNF-TrkB early endocytic trafficking and signaling from early endosomes. Mol. Biol. Cell *22*, 3684–3698.

Fujimura, N. (2016). WNT/β-Catenin Signaling in Vertebrate Eye Development. Front Cell Dev Biol *4*, 138.

Greene, M.J., Kim, J.S., Seung, H.S., EyeWirers (2016). Analogous Convergence of Sustained and Transient Inputs in Parallel On and Off Pathways for Retinal Motion Computation. Cell Rep *14*, 1892–1900.

Ha, S., Stottmann, R.W., Furley, A.J., and Beier, D.R. (2015). A forward genetic screen in mice identifies mutants with abnormal cortical patterning. Cereb. Cortex *25*, 167–179.

Halford, M.M., Armes, J., Buchert, M., Meskenaite, V., Grail, D., Hibbs, M.L., Wilks, A.F., Farlie, P.G., Newgreen, D.F., Hovens, C.M., et al. (2000). Ryk-deficient mice exhibit craniofacial defects associated with perturbed Eph receptor crosstalk. Nat. Genet. *25*, 414–418.

Hall, A.C., Lucas, F.R., and Salinas, P.C. (2000). Axonal remodeling and synaptic differentiation in the cerebellum is regulated by WNT-7a signaling. Cell *100*, 525–535.

Haverkamp, S., and Wässle, H. (2000). Immunocytochemical analysis of the mouse retina. The Journal of Comparative Neurology *424*, 1–23

He, X., Saint-Jeannet, J.P., Wang, Y., Nathans, J., Dawid, I., and Varmus, H. (1997). A member of the Frizzled protein family mediating axis induction by Wnt-5A. Science *275*, 1652–1654.

Heidenreich, M., and Zhang, F. (2016). Applications of CRISPR-Cas systems in neuroscience. Nat. Rev. Neurosci. *17*, 36–44.

Hinds, J.W., and Hinds, P.L. (1979). Differentiation of photoreceptors and horizontal

cells in the embryonic mouse retina: an electron microscopic, serial section analysis. The Journal of Comparative Neurology *187*, 495–511.

Holkers, M., Maggio, I., Henriques, S.F.D., Janssen, J.M., Cathomen, T., and Gonçalves, M.A.F.V. (2014). Adenoviral vector DNA for accurate genome editing with engineered nucleases. Nat. Methods *11*, 1051–1057.

Hollis, E.R., Ishiko, N., Yu, T., Lu, C.-C., Haimovich, A., Tolentino, K., Richman, A., Tury, A., Wang, S.-H., Pessian, M., et al. (2016). Ryk controls remapping of motor cortex during functional recovery after spinal cord injury. Nat. Neurosci. *19*, 697–705.

Hoon, M., Okawa, H., Santina, Della, L., and Wong, R.O.L. (2014). Functional architecture of the retina: development and disease. Prog Retin Eye Res *42*, 44–84.

Hsu, P.D., Scott, D.A., Weinstein, J.A., Ran, F.A., Konermann, S., Agarwala, V., Li, Y., Fine, E.J., Wu, X., Shalem, O., et al. (2013). DNA targeting specificity of RNA-guided Cas9 nucleases. Nature Biotechnology *31*, 827–832.

Huckfeldt, R.M., Schubert, T., Morgan, J.L., Godinho, L., Di Cristo, G., Huang, Z.J., and Wong, R.O.L. (2009). Transient neurites of retinal horizontal cells exhibit columnar tiling via homotypic interactions. Nat. Neurosci. *12*, 35–43.

Jeon, C.J., Strettoi, E., and Masland, R.H. (1998). The major cell populations of the mouse retina. Journal of Neuroscience *18*, 8936–8946.

Kalashnikova, E., Lorca, R.A., Kaur, I., Barisone, G.A., Li, B., Ishimaru, T., Trimmer, J.S., Mohapatra, D.P., and Díaz, E. (2010). SynDIG1: an activity-regulated, AMPA-receptor-interacting transmembrane protein that regulates excitatory synapse development. Neuron *65*, 80–93.

Kang, M.-I., Baker, A.R., Dextras, C.R., Cabarcas, S.M., Young, M.R., and Colburn, N.H. (2012). Targeting of Noncanonical Wnt5a Signaling by AP-1 Blocker Dominant-Negative Jun When It Inhibits Skin Carcinogenesis. Genes Cancer *3*, 37–50.

Katoh, K., Omori, Y., Onishi, A., Sato, S., Kondo, M., and Furukawa, T. (2010). Blimp1 suppresses Chx10 expression in differentiating retinal photoreceptor precursors to ensure proper photoreceptor development. J. Neurosci. *30*, 6515–6526.

Kay, J.N., Chu, M.W., and Sanes, J.R. (2012). MEGF10 and MEGF11 mediate homotypic interactions required for mosaic spacing of retinal neurons. Nature *483*, 465–469.

Keeble, T.R., Halford, M.M., Seaman, C., Kee, N., Macheda, M., Anderson, R.B., Stacker, S.A., and Cooper, H.M. (2006). The Wnt receptor Ryk is required for Wnt5a-mediated axon guidance on the contralateral side of the corpus callosum. J. Neurosci. *26*, 5840–5848.

Kim, G.-H., Her, J.-H., and Han, J.-K. (2008). Ryk cooperates with Frizzled 7 to promote Wnt11-mediated endocytosis and is essential for Xenopus laevis convergent extension movements. J. Cell Biol. *182*, 1073–1082.

Kim, J.-W., Yang, H.-J., Brooks, M.J., Zelinger, L., Karakülah, G., Gotoh, N., Boleda, A., Gieser, L., Giuste, F., Whitaker, D.T., et al. (2016). NRL-Regulated Transcriptome Dynamics of Developing Rod Photoreceptors. Cell Rep *17*, 2460–2473.

Klassen, M.P., and Shen, K. (2007). Wnt signaling positions neuromuscular connectivity by inhibiting synapse formation in C. elegans. Cell *130*, 704–716.

Koike-Yusa, H., Li, Y., Tan, E.-P., Velasco-Herrera, M.D.C., and Yusa, K. (2014). Genome-wide recessive genetic screening in mammalian cells with a lentiviral CRISPR-guide RNA library. Nature Biotechnology *32*, 267–273.

Kolodkin, A.L., and Tessier-Lavigne, M. (2011). Mechanisms and molecules of neuronal wiring: a primer. Cold Spring Harbor Perspectives in Biology *3*, a001727–a001727.

Koso, H., Minami, C., Tabata, Y., Inoue, M., Sasaki, E., Satoh, S., and Watanabe, S. (2009). CD73, a novel cell surface antigen that characterizes retinal photoreceptor precursor cells. Invest. Ophthalmol. Vis. Sci. *50*, 5411–5418.

Koulen, P., Fletcher, E.L., Craven, S.E., Bredt, D.S., and Wässle, H. (1998). Immunocytochemical localization of the postsynaptic density protein PSD-95 in the mammalian retina. Journal of Neuroscience *18*, 10136–10149.

Lakowski, J., Han, Y.-T., Pearson, R.A., Gonzalez-Cordero, A., West, E.L., Gualdoni, S., Barber, A.C., Hubank, M., Ali, R.R., and Sowden, J.C. (2011). Effective transplantation of photoreceptor precursor cells selected via cell surface antigen expression. Stem Cells *29*, 1391–1404.

Le, Y.-Z., Ash, J.D., Al-Ubaidi, M.R., Chen, Y., Ma, J.-X., and Anderson, R.E. (2004). Targeted expression of Cre recombinase to cone photoreceptors in transgenic mice. Mol. Vis. *10*, 1011–1018.

Li, S., Chen, D., Sauvé, Y., McCandless, J., Chen, Y.-J., and Chen, C.-K. (2005). Rhodopsin-iCre transgenic mouse line for Cre-mediated rod-specific gene targeting. Genesis *41*, 73–80.

Lijam, N., Paylor, R., McDonald, M.P., Crawley, J.N., Deng, C.X., Herrup, K., Stevens, K.E., Maccaferri, G., McBain, C.J., Sussman, D.J., et al. (1997). Social interaction and sensorimotor gating abnormalities in mice lacking Dvl1. Cell *90*, 895–905.

Lin, S., Baye, L.M., Westfall, T.A., and Slusarski, D.C. (2010). Wnt5b-Ryk pathway provides directional signals to regulate gastrulation movement. J. Cell Biol. *190*, 263–278.

Linhoff, M.W., Laurén, J., Cassidy, R.M., Dobie, F.A., Takahashi, H., Nygaard, H.B., Airaksinen, M.S., Strittmatter, S.M., and Craig, A.M. (2009). An unbiased expression screen for synaptogenic proteins identifies the LRRTM protein family as synaptic organizers. Neuron *61*, 734–749.

Liu, Y., Shi, J., Lu, C.-C., Wang, Z.-B., Lyuksyutova, A.I., Song, X.-J., Song, X., and Zou, Y. (2005). Ryk-mediated Wnt repulsion regulates posterior-directed growth of corticospinal tract. Nat. Neurosci. *8*, 1151–1159.

Lu, W., Yamamoto, V., Ortega, B., and Baltimore, D. (2004). Mammalian Ryk is a Wnt coreceptor required for stimulation of neurite outgrowth. Cell *119*, 97–108.

Macosko, E.Z., Basu, A., Satija, R., Nemesh, J., Shekhar, K., Goldman, M., Tirosh, I., Bialas, A.R., Kamitaki, N., Martersteck, E.M., et al. (2015). Highly Parallel Genome-wide Expression Profiling of Individual Cells Using Nanoliter Droplets. Cell *161*, 1202–1214.

Matsuda, T., and Cepko, C.L. (2004). Electroporation and RNA interference in the rodent retina in vivo and in vitro. Proc. Natl. Acad. Sci. U.S.a. *101*, 16–22.

Matsuda, T., and Cepko, C.L. (2007). Controlled expression of transgenes introduced by in vivo electroporation. Proc. Natl. Acad. Sci. U.S.a. *104*, 1027–1032.

Matsuoka, R.L., Jiang, Z., Samuels, I.S., Nguyen-Ba-Charvet, K.T., Sun, L.O., Peachey, N.S., Chédotal, A., Yau, K.-W., and Kolodkin, A.L. (2012). Guidance-cue control of horizontal cell morphology, lamination, and synapse formation in the mammalian outer retina. J. Neurosci. *32*, 6859–6868.

Maurel, P., Rauch, U., Flad, M., Margolis, R.K., and Margolis, R.U. (1994). Phosphacan, a chondroitin sulfate proteoglycan of brain that interacts with neurons and neural cell-adhesion molecules, is an extracellular variant of a receptor-type protein tyrosine phosphatase. Proc. Natl. Acad. Sci. U.S.a. *91*, 2512–2516.

Mears, A.J., Kondo, M., Swain, P.K., Takada, Y., Bush, R.A., Saunders, T.L., Sieving, P.A., and Swaroop, A. (2001). Nrl is required for rod photoreceptor development. Nat. Genet. *29*, 447–452.

Merte, J., Wang, Q., Vander Kooi, C.W., Sarsfield, S., Leahy, D.J., Kolodkin, A.L., and Ginty, D.D. (2010). A forward genetic screen in mice identifies Sema3A(K108N), which binds to neuropilin-1 but cannot signal. J. Neurosci. *30*, 5767–5775.

Morgan, J.L., Dhingra, A., Vardi, N., and Wong, R.O.L. (2006). Axons and dendrites originate from neuroepithelial-like processes of retinal bipolar cells. Nat. Neurosci. *9*, 85–92.

Morgans, C.W., Ren, G., and Akileswaran, L. (2006). Localization of nyctalopin in the mammalian retina. Eur. J. Neurosci. Morgans, C.W., Ren, G., and Akileswaran, L. (2006). Localization of nyctalopin in the mammalian retina. Eur. J. Neurosci. Morgans, C.W., Ren, G., and Akileswaran, L. (2006). Localization of nyctalopin in the mammalian retina. Eur. J. Neurosci. *23*, 1163–1171.

Nakamoto, M., Cheng, H.J., Friedman, G.C., McLaughlin, T., Hansen, M.J., Yoon, C.H., O'Leary, D.D., and Flanagan, J.G. (1996). Topographically specific effects of ELF-1 on retinal axon guidance in vitro and retinal axon mapping in vivo. Cell *86*, 755–766.

Olney, J.W. (1968). An electron microscopic study of synapse formation, receptor outer segment development, and other aspects of developing mouse retina. Invest Ophthalmol *7*, 250–268.

Pang, J.-J., Gao, F., Lem, J., Bramblett, D.E., Paul, D.L., and Wu, S.M. (2010). Direct rod input to cone BCs and direct cone input to rod BCs challenge the traditional view of

mammalian BC circuitry. Proc. Natl. Acad. Sci. U.S.a. *107*, 395–400.

Puthussery, T., Gayet-Primo, J., and Taylor, W.R. (2010). Localization of the calcium-binding protein secretagogin in cone bipolar cells of the mammalian retina. Journal of Comparative Neurology *518*, 513–525.

Ran, F.A., Hsu, P.D., Wright, J., Agarwala, V., Scott, D.A., and Zhang, F. (2013). Genome engineering using the CRISPR-Cas9 system. Nat Protoc *8*, 2281–2308.

Rehemtulla, A., Warwar, R., Kumar, R., Ji, X., Zack, D.J., and Swaroop, A. (1996). The basic motif-leucine zipper transcription factor Nrl can positively regulate rhodopsin gene expression. Proc. Natl. Acad. Sci. U.S.a. *93*, 191–195.

Ribic, A., Liu, X., Crair, M.C., and Biederer, T. (2014). Structural organization and function of mouse photoreceptor ribbon synapses involve the immunoglobulin protein synaptic cell adhesion molecule 1. Journal of Comparative Neurology *522*, 900–920.

Rich, K.A., Zhan, Y., and Blanks, J.C. (1997). Migration and synaptogenesis of cone photoreceptors in the developing mouse retina. The Journal of Comparative Neurology *388*, 47–63.

Robinson, M.D., McCarthy, D.J., and Smyth, G.K. (2010). edgeR: a Bioconductor package for differential expression analysis of digital gene expression data. Bioinformatics *26*, 139–140.

Roesch, K., Jadhav, A.P., Trimarchi, J.M., Stadler, M.B., Roska, B., Sun, B.B., and Cepko, C.L. (2008). The transcriptome of retinal Müller glial cells. Journal of Comparative Neurology *509*, 225–238.

Rowan, S., and Cepko, C.L. (2004). Genetic analysis of the homeodomain transcription factor Chx10 in the retina using a novel multifunctional BAC transgenic mouse reporter. Dev. Biol. *271*, 388–402.

Rubinson, D.A., Dillon, C.P., Kwiatkowski, A.V., Sievers, C., Yang, L., Kopinja, J., Rooney, D.L., Zhang, M., Ihrig, M.M., McManus, M.T., et al. (2003). A lentivirus-based system to functionally silence genes in primary mammalian cells, stem cells and transgenic mice by RNA interference. Nat. Genet. *33*, 401–406.

Sakuma, T., Nishikawa, A., Kume, S., Chayama, K., and Yamamoto, T. (2014). Multiplex genome engineering in human cells using all-in-one CRISPR/Cas9 vector system. Scientific Reports *4*.

Samuel, M.A., Voinescu, P.E., Lilley, B.N., de Cabo, R., Foretz, M., Viollet, B., Pawlyk, B., Sandberg, M.A., Vavvas, D.G., and Sanes, J.R. (2014). LKB1 and AMPK regulate synaptic remodeling in old age. Nat. Neurosci. *17*, 1190–1197.

Sanes, J.R., and Zipursky, S.L. (2010). Design principles of insect and vertebrate visual systems. Neuron *66*, 15–36.

Scheiffele, P., Fan, J., Choih, J., Fetter, R., and Serafini, T. (2000). Neuroligin expressed in nonneuronal cells triggers presynaptic development in contacting axons. Cell *101*,

657–669.

Schnitzer, J., and Rusoff, A.C. (1984). Horizontal cells of the mouse retina contain glutamic acid decarboxylase-like immunoreactivity during early developmental stages. Journal of Neuroscience *4*, 2948–2955.

Serafini, T., Kennedy, T.E., Galko, M.J., Mirzayan, C., Jessell, T.M., and Tessier-Lavigne, M. (1994). The netrins define a family of axon outgrowth-promoting proteins homologous to C. elegans UNC-6. Cell *78*, 409–424.

Shalem, O., Sanjana, N.E., Hartenian, E., Shi, X., Scott, D.A., Mikkelsen, T.S., Heckl, D., Ebert, B.L., Root, D.E., Doench, J.G., et al. (2014). Genome-scale CRISPR-Cas9 knockout screening in human cells. Science *343*, 84–87.

Shekhar, K., Lapan, S.W., Whitney, I.E., Tran, N.M., Macosko, E.Z., Kowalczyk, M., Adiconis, X., Levin, J.Z., Nemesh, J., Goldman, M., et al. (2016). Comprehensive Classification of Retinal Bipolar Neurons by Single-Cell Transcriptomics. Cell *166*, 1308–1323.e1330.

Sherry, D.M., Wang, M.M., Bates, J., and Frishman, L.J. (2003). Expression of vesicular glutamate transporter 1 in the mouse retina reveals temporal ordering in development of rod vs. cone and ON vs. OFF circuits. The Journal of Comparative Neurology *465*, 480–498.

Shinmyo, Y., Tanaka, S., Tsunoda, S., Hosomichi, K., Tajima, A., and Kawasaki, H. (2016). CRISPR/Cas9-mediated gene knockout in the mouse brain using in utero electroporation. Scientific Reports *6*, 20611.

Siegert, S., Cabuy, E., Scherf, B.G., Kohler, H., Panda, S., Le, Y.-Z., Fehling, H.J., Gaidatzis, D., Stadler, M.B., and Roska, B. (2012). Transcriptional code and disease map for adult retinal cell types. Nat. Neurosci. *15*, 487–95–S1–2.

Soto, F., Watkins, K.L., Johnson, R.E., Schottler, F., and Kerschensteiner, D. (2013). NGL-2 Regulates Pathway-Specific Neurite Growth and Lamination, Synapse Formation, and Signal Transmission in the Retina. Journal of Neuroscience *33*, 11949–11959.

Swiech, L., Heidenreich, M., Banerjee, A., Habib, N., Li, Y., Trombetta, J., Sur, M., and Zhang, F. (2015). In vivo interrogation of gene function in the mammalian brain using CRISPR-Cas9. Nature Biotechnology *33*, 102–106.

Uezu, A., Kanak, D.J., Bradshaw, T.W.A., Soderblom, E.J., Catavero, C.M., Burette, A.C., Weinberg, R.J., and Soderling, S.H. (2016). Identification of an elaborate complex mediating postsynaptic inhibition. Science *353*, 1123–1129.

Umbhauer, M., Djiane, A., Goisset, C., Penzo-Méndez, A., Riou, J.F., Boucaut, J.C., and Shi, D.L. (2000). The C-terminal cytoplasmic Lys-thr-X-X-X-Trp motif in frizzled receptors mediates Wnt/beta-catenin signalling. Embo J. *19*, 4944–4954.

Umemori, H., Linhoff, M.W., Ornitz, D.M., and Sanes, J.R. (2004). FGF22 and its close relatives are presynaptic organizing molecules in the mammalian brain. Cell *118*, 257–

270.

Vactor, D.V., Sink, H., Fambrough, D., Tsoo, R., and Goodman, C.S. (1993). Genes that control neuromuscular specificity in Drosophila. Cell *73*, 1137–1153.

van Wyk, M., Hulliger, E.C., Girod, L., Ebneter, A., and Kleinlogel, S. (2017). Present Molecular Limitations of ON-Bipolar Cell Targeted Gene Therapy. Front Neurosci *11*, 161.

Veleri, S., Nellissery, J., Mishra, B., Manjunath, S.H., Brooks, M.J., Dong, L., Nagashima, K., Qian, H., Gao, C., Sergeev, Y.V., et al. (2017). REEP6 mediates trafficking of a subset of Clathrin-coated vesicles and is critical for rod photoreceptor function and survival. Hum. Mol. Genet. Veleri, S., Nellissery, J., Mishra, B., Manjunath, S.H., Brooks, M.J., Dong, L., Nagashima, K., Qian, H., Gao, C., Sergeev, Y.V., et al. (2017). REEP6 mediates trafficking of a subset of Clathrin-coated vesicles and is critical for rod photoreceptor function and survival. Hum. Mol. Genet. Veleri, S., Nellissery, J., Mishra, B., Manjunath, S.H., Brooks, M.J., Dong, L., Nagashima, K., Qian, H., Gao, C., Sergeev, Y.V., et al. (2017). REEP6 mediates trafficking of a subset of Clathrin-coated vesicles and is critical for rod photoreceptor function and survival. Hum. Mol. Genet. *26*, 2218–2230.

Wang, S., Sengel, C., Emerson, M.M., and Cepko, C.L. (2014). A gene regulatory network controls the binary fate decision of rod and bipolar cells in the vertebrate retina. Dev. Cell *30*, 513–527.

Wang, T., Lander, E.S., and Sabatini, D.M. (2016). Viral Packaging and Cell Culture for CRISPR-Based Screens. Cold Spring Harb Protoc *2016*, pdb.prot090811.

Wässle, H., Puller, C., Müller, F., and Haverkamp, S. (2009). Cone contacts, mosaics, and territories of bipolar cells in the mouse retina. J. Neurosci. *29*, 106–117.

Witze ES, Litman ES, Argast GM, Moon RT, Ahn NG. (2008) Wnt5a control of cell polarity and directional movement by polarized redistribution of adhesion receptors. Science. 320, 365-9.

Wright, K.M., Lyon, K.A., Leung, H., Leahy, D.J., Ma, L., and Ginty, D.D. (2012). Dystroglycan organizes axon guidance cue localization and axonal pathfinding. Neuron *76*, 931–944.

Yamagata, M., and Sanes, J.R. (2012). Expanding the Ig superfamily code for laminar specificity in retina: expression and role of contactins. J. Neurosci. *32*, 14402–14414.

Yamagata, M., Weiner, J.A., and Sanes, J.R. (2002). Sidekicks: synaptic adhesion molecules that promote lamina-specific connectivity in the retina. Cell *110*, 649–660.

Yao, R., Natsume, Y., and Noda, T. (2004). MAGI-3 is involved in the regulation of the JNK signaling pathway as a scaffold protein for frizzled and Ltap. Oncogene *23*, 6023–6030.

Young, R.W. (1985). Cell differentiation in the retina of the mouse. Anat. Rec. *212*, 199–

205.

Yu, H., Ye, X., Guo, N., and Nathans, J. (2012). Frizzled 2 and frizzled 7 function redundantly in convergent extension and closure of the ventricular septum and palate: evidence for a network of interacting genes. Development *139*, 4383–4394.

Yu, W., Mookherjee, S., Chaitankar, V., Hiriyanna, S., Kim, J.-W., Brooks, M., Ataeijannati, Y., Sun, X., Dong, L., Li, T., et al. (2017). Nrl knockdown by AAV-delivered CRISPR/Cas9 prevents retinal degeneration in mice. Nat Commun *8*, 14716.

Yue, Q., Wagstaff, L., Yang, X., Weijer, C., and Münsterberg, A. (2008). Wnt3a-mediated chemorepulsion controls movement patterns of cardiac progenitors and requires RhoA function. Development *135*, 1029–1037.

Zhang, C., Kolodkin, A.L., Wong, R.O., and James, R.E. (2017). Establishing Wiring Specificity in Visual System Circuits: From the Retina to the Brain. Annu. Rev. Neurosci. *40*, annurev–neuro–072116–031607.

FIGURE LEGENDS:

Figure 1. Development of the OPL

A. Schematic of the adult retina.

B. Generation of the OPL. Rods (anti-Rhodopsin) and cones (anti-S-opsin) are present at P2; additional rods form after P2. At P4-5, gaps between the nuclear layers coincides with photoreceptor terminals in the presumptive OPL (arrowhead). By P6-8, the OPL is continuous (arrowhead). Nuclei labeled with TOPRO3 and HCs with calbindin; left and center panels show the same fields and are maximum projections. Scale bar, 10 μm.

C. Synaptogenesis. Sparsely labeled cone terminals (Hb9:GFP transgene) are visible by P4. Juxtaposition of the presynaptic marker Bassoon and the postsynaptic marker mGluR6 first appears in cones (white arrowheads) at P7 and in rods (yellow arrowheads) by P13. Scale bar, 10 μm.

D. Segregation of rod and cone terminal layers. Dendrites of cone bipolars (anti-Scgn) and rod bipolars (anti-PKC) overlap at early stages (P9) as do rod (anti-PSD-95) and cone (anti-CAR) terminals. Rod and cone synapses segregate into separate layers between P13 and P21 (sublaminar boundary represented by dotted lines). Although PSD-95 is

expressed by both rods and cones, its uniquely focal localization in rod terminals allowed us to use it as a marker for rod terminal positioning. Scale bar, 10 µm.

See also Figure S1.

Figure 2. Cellular rearrangements during OPL development

A, B. Rod somata are transiently present in the developing INL. Rod somata (anti-Rhodopsin) are present below the developing OPL until P7. By P9, INL cells juxtaposing the OPL are BCs (anti-Chx10). Nuclei labeled with TOPRO3. Scale bar, 10 µm.

C. Secondary HC processes (anti-Calbindin) appear at P5 and join the OPL by P7. Rod somata (anti-Rhodopsin) are initially intermingled with those of HCs (P1), then also found between the HC processes (P5) as shown by arrows, and finally exclusive to the ONL (P7, P9). Scale bar, 10 µm.

D. The ONL gains an equal amount of rod somata as are lost from INL. This is consistent with rods migrating from the distal INL across the OPL into the ONL. Error bars = Standard error. Thickness determined in cross-section, n=3 for each measurement.

E. Overview of OPL development, summarizing data from Figure 1 B-D.

F. Overview of cellular rearrangements during OPL development, summarizing data from panels A-D.

Figure 3: Analysis of RNA sequencing data

A. Number of Differentially Expressed (DE) genes across time points and between cell types are shown with arrows indicating the direction of enrichment (see Table S4). DE genes were identified at FDR 5% with a minimum fold change cut-off greater than 4 (see *Methods*). Asterisk denotes significant overrepresentation of genes associated with gene ontology term “plasma membrane”. Total genes analyzed = 13812.

B. Identification of cell surface and secreted proteins (see *Methods*). Annotation was performed on merged DE gene list identified in all pairwise comparisons (Figure 2A).

C. Cell surface and secreted proteins (CSPs) differentially enriched in rods and cones, and between rod bipolar cells (RBC) and cone bipolar cells (CBC) at P13. Expression values are shown as mean logCPM (log2-Counts Per Million) of the two biological replicates. Genes are ordered by fold change.

D. Expression patterns of differentially expressed cell surface proteins of selected protein families at P13. LRR = Leucine Rich Repeat, PTP = Protein Receptor Tyrosine Phosphatases, and IG = immunoglobulin-superfamily proteins. Z-scores are plotted for each gene.

E. Comparison of RBC and CBC enriched cell surface and secreted proteins (CSPs) with ON bipolar types (BC5-9) from single cell DropSeq data (Shekhar et al., 2016). For each type, we show the number of RBC- or CBC-enriched CSPs that were also detected by DropSeq in at least 5% of cells. See *Methods* and Figure S2B for details.

See also Figures S2, S3

Figure 4: CRISPR/Cas9 Gene knockout in the postnatal retina.

A. Schematic of CRISPR-Cas9 knock out vectors. Guide RNAs (sgRNAs) are cloned downstream of the U6 RNA Polymerase III promoter. Three vectors were used, in which Cas9 and GFP were expressed either separately (px330) or together (px458), or one (px330, px458) or two sgRNAs were expressed simultaneously (px458 multi). DNA (shown in green) is injected into the subretinal space of newborn CD1 (albino) pups and delivered into dividing cells via electroporation.

B. Conversion of rods to cone-like cells (cods) via Nrl-CRISPR. Image shows rods electroporated with a single plasmid bearing *Nrl*^{sgRNA} + *Cas9* + *GFP*. These transformed cells (green) express a cone specific opsin (S-opsin; red cells). By contrast, transfected control cells do not express S-opsin (i.e. no yellow cells). In addition, cod axon terminals terminate in the cone layer of the OPL (sublaminar boundaries represented by dotted lines), display enhanced clustering of a postsynaptic marker (stained with Cacna1), and form contacts to cone bipolars (stained with Scgn). Terminal fate marker images are maximum projections. Scale bar, 10µm.

C. S-opsin immunoreactivity of cells electroporated with constructs that attenuate Nrl function. Dominant negative: a transgene encoding a dominant negative version of Nrl; shRNA: transgene expressing an shRNA directed towards Nrl; CRISPR: CRISPR-Cas9 and gRNA directed toward Nrl on a separate plasmid from GFP; CRISPR2 Cas9 T2A GFP: all transgenes (gRNA, Cas9 and GFP) on the same plasmid.

D. Loss of mGluR6 protein (red) juxtaposing terminals of rods (dotted circles) transfected with an Elfn1 CRISPR (GFP; green). Scale bar, 10µm.

E. Knockout of Prkca (PKC) in rod bipolar cells and Secretagogin (Scgn) in cone bipolar cells (arrowheads). Cas9 was expressed from a mGluR6 promoter. See Figure S4C for quantification. Retinas were examined at P9. Scale bar, 10µm.

F. Rods were converted to cods via an Nrl-directed gRNA (CRISPR2 as in B), and a second gene was targeted by a separate gRNA encoded on the same plasmid. Left: Knock out efficiencies for co-electroporation of two CRISPR-bearing vectors and for a single vector bearing both sgRNAs. Charts represent average values scored for at least 3 animals under each condition. Right: Photoreceptor terminals electroporated with multiplexed Crispr vectors with gRNAs directed towards Nrl and Bassoon. Red arrow, a cell in which only Nrl, but not Bassoon, was knocked out. Green arrow, a cell in which only Bassoon was knocked out; Yellow arrow, both Nrl and Bassoon were knocked out. Scale bar = 10µm.

G. Mutations differentially effect sprouting of neurites. Cells transfected with a Bassoon CRISPR (middle row) show retraction of rod terminals (PSD-95), sprouting of RBCs (PKC), CBCs (SCGN), and horizontal cells (CALB) but no cone defects (CAR). Those transfected with a Cadm1 CRISPR (bottom panel) show only horizontal cell sprouting (CALB). Cells transfected with the Control CRISPR (no sgRNA) show neither retraction nor sprouting (top panel). Panels showing cell-type marker expression are zoomed regions of red dotted boxes. Images are maximum projections. Scale bar, 10µm.

See also Figures S4

Figure 5: Several CRISPR/Cas9-based mosaic knockouts disrupt development of the outer retina.

A. Enlarged rod terminals in *Gpc-2*^{CRISPR} animals. Images show rods electroporated with px458 harboring the *Gpc-2* sgRNA. Rod terminals are labeled with PSD-95 (red). Scale bar, 10µm. Right: quantification. Significance is determined by single-tailed Student's t-test (** = p<0.01, * = p<.05).

B. Misplaced rod terminals in *Wisp-1*^{CRISPR} animals. Images show rods (green) electroporated with px458 harboring the *Wisp-1* sgRNA. Cone terminals are labeled with Cone arrestin (red). White dotted lines demarcate the OPL region populated with rod terminals – i.e., the rod sublamina. A rod soma is labeled with a white star. Scale bar, 10µm. Right: quantification, see *Methods* for further details on phenotyping. Significance is determined by single-tailed Student's t-test (** = p<0.01).

C. HC sprouting in *Tmem108*^{CRISPR} animals. Images (maximum projections) show rods electroporated with px458 harboring the *Tmem108* sgRNA. HCs are labeled with anti-Calbindin (CALB, white). Scale bar, 10µm. Right: quantification, see *Methods* for further details on phenotyping. Significance is determined by single-tailed Student's t-test (** = p<0.01).

D. Ectopic PSD-95 expression and HC sprouting in *Ptprz1*^{CRISPR} animals. Images are maximum projections showing rods electroporated with px458 harboring the *Ptprz1* sgRNA. HCs are labeled with anti-Calbindin (CALB, red) and photoreceptor terminals are labeled with anti-PSD-95 (white). Scale bar, 10µm. Right: quantification; counts refer to number of PSD-95 puncta or HC sprouts, see *Methods* for further details on phenotyping. *Ptprz1*^{CRISPR} represents average counts of two CRISPRs. Right panel is the zoomed region of white dotted box. Significance is determined by single-tailed Student's t-test (* = p<0.05).

Figure 6:

CRISPR-Cas9 mediated knockout of Wnt5 induces a second OPL

A. Expression patterns of Wnt pathway components in rods, cones, RBCs and CBCs at P13. Values are shown as mean logCPM (log2-Counts Per Million).

B. CRISPR double knock out of Wnt5a/5b, and single knock outs of Dvl1 induce a second neuropil in the outer retina. Retinas were assayed at P21. GFP, electroporated cells; anti-PSD-95, photoreceptor terminals; TOPRO3, nuclei. Controls (left panels), were electroporated with an empty CRISPR vector. Scale bar, 10 μm.

C. Composition of the ectopic neuropil in Wnt5a/5b CRISPR-knockout retinas. In addition to rod terminals, the ectopic neuropil contains cone axon terminals and processes of horizontal cells, CBCs, and RBCs. Retinas stained at P21. Markers: Electroporated cells (GFP), Horizontal cells (anti-Calbindin), Cones (anti-Cone Arrestin), CBCs (anti-Secretagogin), and RBCs (anti-PKC). Scale bar, 10μm.

D. Synapses are formed in the ectopic OPL: Retinas were stained with antibodies to Bassoon, a presynaptic protein in photoreceptor terminals, and to mGluR6, a postsynaptic marker in ON bipolar cells. Bassoon and mGluR6 puncta remain juxtaposed in the Wnt5a/b^{CRISPR}-induced ectopic OPL, indicating close apposition of pre- and postsynaptic structures. Scale bar, 10μm.

See also Figure S5, S6

Figure 7:

Wnt5 acts through the Ryk-dependent pathway

A. CRISPR knockouts of non-canonical Wnt receptor Ryk or of both Fzd4 and Fzd5 phenocopied Wnt5a/5b knockouts. In contrast, neither knockouts of Fzd4 or Fzd5 individually, nor genetic disruption of the canonical Wnt pathway (Lrp6 knockout or Dkk1 overexpression) displayed abnormalities. Three to six retinas analyzed per mutant. Markers used: anti-PSD-95, photoreceptor terminals; anti-GFP, electroporated patches; and TOPRO3, nuclear marker. Scale bar, 10μm.

B. The ectopic OPL stained for processes of Rod Bipolar Cells (anti-PKC), Horizontal Cells (anti-Calbindin (Calb)), Cone Bipolar Cells (anti-Secretagogin (Scgn)), and Cones (anti-Cone Arrestin (CAR)) in addition to rod terminals (middle panels; anti-PSD-95). White arrows indicate cone terminals within Ryk CRISPR-induced lamina. Scale bar, 10μm.

C. Ectopic laminae were observed as early as P6 in both CRISPR-mediated knock outs of Ryk and double knockouts of Wnt5a/5b. Markers: OPL, anti-PSD-95; transfected cells, GFP; and nuclei, TOPRO3. Scale bar, 10μm.

D. A second neuropil was formed when Ryk was knocked out of rods by targeting Cas9 expression using the Rhodopsin promoter (Rod^{prom}), but not when targeting to bipolar cells (BC^{prom}). Markers: OPL, anti-PSD-95; electroporated cells, anti-GFP. Likewise, a duplicated OPL was observed when Dvl1 knockout was limited to rods but not to bipolar cells. Scale bar, 10 μm.

E. Three day retina cultures grown in bath-applied BSA, Wnt5A (Figure S7), Wnt5B (Figure S7) or Wnt5A/5B. Wnt ligands were bath applied at a total concentration of 100 ng/mL (For Wnt5a/5b, 50 ng/mL each). Rods were distinguished by cell type specific antibodies against Rhodopsin. Nuclei were stained with DAPI (blue). Scale bar, 10 μm.

F. (Left) Quantification of D. From left to right: n (cells/cultures) = 64/4, 56/4, 70/2, 57/2. (Right) Quantification of neurite outgrowth in control and Ryk knockout cultured rods. Wnt5a and Wnt5b were bath applied at a concentration of 100ng/mL. From left to right: n (cells/cultures) = 34/2, 41/2, 39/2. Significance determined by two-tailed Student's T-test comparison between test condition and control (BSA). *** = p<.001; n.s. = not significant.

G. Conditional germline knockout of Ryk phenocopies Ryk^{CRISPR}. Knockout was targeted to rods using the Rho-icre transgenic line. $Ryk^{flox/flox}$ animals were first crossed to Ai14 transgenic mice and then to the Rho-icre line. Markers: OPL, anti-PSD-95 (green), rods: anti-dsRed, Cre-dependent TdTom, Nuclei: TOPRO-3. Scale bar, 10 μm.

H. Germline knockouts of Dvl1 phenocopy $Dvl1^{CRISPR}$. Markers: OPL, anti-PSD-95; rods, anti-Reep6; Nuclei, TOPRO-3. Scale bar, 10 μm.

I. Summary of Wnt signaling pathway elucidated from experiments shown in Figs. 6,7.

See also Figures S6, S7.

Supplementary Figures:

Figure S1. Related to Figure 1,2. OPL development

A. Outer retinal organization prior to OPL formation. Cones (S-opsin), HCs (Lim1), Ganglion cells (RBPMS), Nuclei (TOPRO3). Images are maximum projections.

A'. Early born neuronal classes occupy distinct layers prior to the appearance of the OPL but occasional intermixing of cones and horizontal cells is apparent (arrow) in the ONBL (outer nucleoblast layer). Lim1 also labels amacrine cells located near the GCL. Scale bar, 10μm.

A''. Nuclear staining shows no visible OPL. Scale bar, 10μm.

B. Cones (labeled with Hb9:GFP transgene) make multiple contacts with horizontal cell (HCs, labeled with anti-Calbindin) processes as early as postnatal day 3, as shown in Examples 1 and 2. Example 2 also shows a more developed cone, with a bulbous terminal at its HC-contact site (arrow). Images are maximum projections. Scale bar, 10μm.

C. Bipolar cell development during synaptogenesis.

C'. P4. Left panel: a single neurite of an ON bipolar cell (Grm6:GFP) spans the future ONL, highlighted with the nuclear stain, DAPI (left panel). Middle panel: Grm6:GFP-expressing cell alone. Right panel: expression of presynaptic (anti-Bassoon) and postsynaptic (anti-mGluR6) protein expression. Scale bar, 10μm.

C''. P7. Left panel: more ON bipolars are present in the INL (Grm6:GFP) with the majority of bipolar processes contained within the OPL (left, middle panels). Right panel shows presynaptic Bassoon (green) widely expressed throughout the OPL, whereas the postsynaptic mGluR6 (red) appears in distinct clusters (arrow). Inset is zoomed region of dotted box in right panel.

Figure S2. Related to Figure 3. Analysis of RNA sequencing data

A. Spearman correlation coefficients between all pairs of RNA sequencing libraries determined from logCPM expression values.

B. Distribution of RBC and CBC enriched cell surface and secreted proteins (CSPs) at P13 among the different subtypes of ON bipolar cells (BC5-9) based on single cell profiling data. Expression values are shown as logCPM for RNA sequencing data (left, from this

study) and as percentage of cells in which CSP was detected for DropSeq data (right, from Shekhar et al., 2016). Genes are ordered by fold change in RNA sequencing data. Total number of genes expressed in DropSeq for each subtype (top row) were defined as being expressed in at least 5% of cells as described in *Methods*.

Figure S3. Related to Figure 3. Differential gene expression of transcription factors, channels, receptors, and transporters.

Expression patterns of transcription factors (A), channels (B), receptors (C), and transporters (D) differentially expressed between rods and cones and between RBCs and CBCs at P13. Values are shown as Z-scores.

Figure S4. Related to Figure 4. CRISPR/Cas9-induced knockouts.

A. Loss of PSD-95 or Bassoon protein in rods electroporated with Cas9+CRISPRs designed to target either locus. In wild-type, Bassoon protein in rod terminals appears as a single dot (arrowhead). This disappears in rods transfected with Bassoon CRISPR. Images show rod terminals electroporated with px458 vector harboring either CRISPR. Green = GFP; Red = anti-PSD-95, White = anti-Bassoon. Scale bar, 10μm. Right: Quantification.

B. Loss of Elfn1 does not disrupt overall organization of the outer retina. Images show antibody-labeled Horizontal cells (Left: CALB, red) or Rod Bipolar cells (Right: PKC, red). Electroporated rods express GFP (green) and nuclei are labeled with DAPI. Images are maximum projections. Scale bar, 10μm.

C, D. Numbers of transfected cells with either Scgn CRISPR or PKC CRISPR that are positive for Scgn (top) or PKC (bottom) protein expression compared to controls. Controls are cells transfected with the CRISPR plasmid lacking a sgRNA sequence. The number of Scgn-positive cells in Scgn CRISPR transfected retinas is significantly reduced; however, the number of PKC-positive cells is not statistically different from controls. Conversely, the number of PKC-positive cells in Prkca CRISPR is significantly reduced whereas there is not statistical difference in Scgn expression compared to controls. **p<0.01; *p<0.05; n.s. = not significant. Significance determined by two-tailed Student's t-test.

E. Cells transfected (GFP, green) with the Nrl CRISPR display cone-like characteristics. Outer segments of cods appear shorter (cone-like) compared to transfected wild-type rods. Further, they express the cone axon terminal marker PNA. Scale bar, 10μm.

F. Comparison of cone-enriched and rod-enriched cell surface and secreted proteins (CSPs) at P13 to wild-type rods (Nrl WT) and Nrl knock out (Nrl KO) cods at P14 (Kim et al., 2016). Values are plotted as log2-fold-change expression values between rods and cones in this study (x-axis) and between Nrl WT and Nrl KO observed in Kim et al., 2016 (y-axis). The cone-enriched Frizzled 10 (Fzd10) is shown in red. CSP expression pattern of cods (Nrl KO) were more similar to cones than to rods. See *Methods* for details.

G. Comparison of knock out efficiencies between co-electroporation of two CRISPR-bearing vectors versus a single vector bearing both sgRNAs. Although expressed more robustly in rods, PSD-95 is also expressed at the base of cone terminals. Nrl^{CRISPR} was either co-electroporated or multiplexed with $Psd\text{-}95^{CRISPR}$. Right: Immunofluorescent images showing photoreceptor terminals electroporated with multiplexed Crispr vectors with gRNAs directed towards Nrl and Psd-95. Red arrow, a cell in which only Nrl, but not Psd-95, was knocked out. Green arrow, a cell in which only Psd-95 was knocked out; Yellow arrow, both Nrl and Psd-95 were knocked out. Scale bars, 10μm.

Figure S5. Related to Figures 6, 7. CRISPR-induced knockouts in cods and developmental expression of Wnt components.

A. CRISPR knockouts of canonical Wnt receptors and enhancers have no effect on OPL positioning. Three to six retinas analyzed per mutant. Markers used: anti-PSD-95 photoreceptor terminals; anti-GFP, electroporated patches; and TOPRO3, nuclear marker. Scale bar, 10μm.

B. Inactivation of Syndig1L, Fzd10 (shown at P21) and Dvl1 (shown at P14) via CRISPR-Cas9 in cods (generated with $Nrl^{CRISPR2}$) results in sprouting of Horizontal cell processes into the INL. By contrast, sprouting of bipolar dendrites was not observed (not shown). Markers: Horizontal cells, anti-calbindin and electroporated cells, GFP. Images are maximum projections. Scale bar = 10μm. See *Methods* further details on phenotyping.

C. Quantification of B. All animals scored at P21. Error bars represent standard error.

D. Quantification of B. All animals scored at P14. Error bars represent standard error.

D. Expression patterns of Wnt pathway components in rods, cones, and bipolars at different time points. Values are shown as mean logCPM (log2-counts-per-million) between the two biological replicates.

Figure S6. Related to Figures 6,7. Expression of Wnt-pathway members across time and development of doubled OPL phenotype.

A-C. Cells in between two OPLs in Ryk^{CRISPR} mutants are rods in that they are positive for Recoverin (Rods + Cones) as shown by red arrows in (B), but not S-opsin (Cones; C), or Chx10 (Bipolars; A). Electroporated cells = green. Insets are zoomed images of white boxed regions. Scale bar = 10μm.

D. Ryk conditional germline knockout and heterozygotes display supernumerary OPLs. Markers: Rod terminals (anti-PSD-95, red), Nuclei (DAPI), Cones (anti-CAR, green). Scale bar = 10 μm.

E. Dvl1 germline knockouts display supernumerary OPLs. Markers: Rod terminals (anti-PSD-95, red), Nuclei (TOPRO3), Cones (anti-CAR, green). Scale bar = 10 μm.

F. Occasional rods are found in the OPL until P8. Markers: Nuclei (TOPRO3), Bipolar cells (anti-Chx10, red). Scale bar = 10 μm.

Figure S7. Related to Figure 6. Cultured rods respond to Wnt5.

A. Three-day retinal cultures grown with bath-applied BSA or Wnt3a. From left to right n (cells/cultures): 30/2, 31/2, 32/2, 35/2. Significance determined by two-tailed Student's T-test comparison between test condition and control (BSA). n.s. = not significant.

B. P3 rods cultured for one day displayed enriched Ryk expression. Faint, punctate staining on all cells is presumed to be background. Rods with *Ryk*^{CRISPR} show reduced levels of Ryk. Rods were co-electroporated (*in vivo*) with two plasmids encoding either Ryk^{CRISPR}/Cas9 or $Control^{CRISPR}$/Cas9 and mCherry at P0, then cultured at P3 for 1 day *in*

vitro. White arrows mark Rhodopsin positive cells. Rho = Rhodopsin, DAPI = nuclei. Scale bar, 10µm.

C. *Ryk*^{CRISPR} reduces RYK expression in cultured rods. Histograms show Ryk signal intensity (normalized to maximum signal within field) for rhodopsin-positive cells that also express mCherry (see Figure 6). Control sgRNA: n=3 cultures, 77 total cells; Ryk sgRNA: n=3 cultures, 84 total cells.

D. Ryk-knockout rods do not respond to Wnt5a/5b. Rods co-electroporated *in vivo* with *mCherry* + *Ryk*^{CRISPR} or Control^{CRISPR} cultured at P3 for 3 days. Wnt5a and Wnt5b were bath applied at a concentration of 100ng/mL. As Ryk knockout was partially penetrant (see B), we compared electroporated cells that either expressed or did not express Ryk. Top inset: mCherry-expressing rod also expresses RYK. Bottom inset: mCherry expressing rod does not express Ryk; a second Ryk (+) mCherry (-) neurite runs in parallel. Right: Quantification of neurite lengths of electroporated rods that continue to express Ryk. From left to right: n (cells/cultures) = 38/2, 41/2, 50/2. Neurite lengths of Ryk knock out rods are quantified in Figure 7D. Significance determined by two-tailed Student's T-test comparison between test condition and control (BSA). *** = p<.001. Scale bar = 10µm.

E. Neurite outgrowth in cultured cones. Cones were distinguished by cell-type specific antibodies against S-opsin (shown in red). Scale bar = 10µm.

F. Quantification of neurite outgrowth in cultured cones. Cones were distinguished by cell-type specific antibodies against S-opsin. From left to right: n (cells/cultures) = 63/4, 79/2, 59/2, 67/2. n.s. = not significant. Significance determined by two-tailed Student's T-test comparison between test condition and control (BSA). n.s. = not significant.

G. Three day retina cultures grown in bath-applied BSA (Figure 6), Wnt5A, or Wnt5B. Wnt ligands were bath applied at a total concentration of 100 ng/mL Rods were distinguished by cell type specific antibodies against Rhodopsin. Nuclei were stained with DAPI (blue). Scale bar, 10 µm.

STAR Methods

CONTACT FOR REAGENT AND RESOURCE SHARING

Further information and requests for reagents may be directed to, and will be fulfilled by the Lead Contact S. Lawrence Zipursky.

EXPERIMENTAL MODEL AND SUBJECT DETAILS

Animals

Mice were handled and tissue obtained following protocols approved by the Harvard University Standing Committee on the Use of Animals in Research and Teaching and the Chancellor's Animal Research Committee (ARC) at UCLA. CD1 mice used for electroporations were obtained from Charles River (Cambridge). P0 indicates the day pups were born. Unless otherwise indicated, pups were electroporated at P0-1 and sacrificed at P21. Males and females were both used for RNA sequencing and electroporation experiments.

The following mouse lines were used in this study:

1. Tg(B6;SJL-Pde6b+ Tg(Rho-icre)1Ck/Boc) to isolate rods (Li et al., 2005) and Tg(OPN1LW-cre)#Yzl) to isolate cones (Le et al., 2004) were kindly provided by Dr. XianJie Yang at UCLA.
2. Tg((Grm6-EGFP)5Var) for sorting bipolar cells (Morgan et al., 2006) were generously provided by Dr. Rachel Wong at University of Washington.
3. Conditional deletion of Ryk crossed into Ai14 trangenic animals (*Ryk*$^{flox/flox}$) were kindly provided by Dr. Yimin Zou at UCSD.
4. Germline knockout of Dvl1 were kindly provided by Anthony Wynshaw-Boris at Case Western Reserve University.

METHOD DETAILS

Sorting Cell Types and Library Construction

LIVE sample preparation (rods, cones, ON bipolars)

Eyes were enucleated from 3 animals and their retinas were dissected. Retinal tissue was collected in HBSS, calcium, magnesium with 10% Fetal Bovine Serum (referred as HBSS+) media. Tissue was spun at 1000rpm for 30 secs and washed twice with HBSS,

no calcium, no magnesium (referred as HBSS-) media. Media was replaced with HBSS- containing 100 units/mL of Papain and 0.18 Wu/mL of Liberase TM. Tissue was incubated at 37°C for 15 min in a microfuge shaker at 1,000 rpm. Cells were mechanically dissociated by pipetting up and down with a P1000 tip at 5 and 10 min into this incubation. At 15 min, digestion was inactivated by addition of HBSS+ media and the sample was treated with 50 ug/mL of DNAse. Further dissociation was performed by passing the sample through a 21G 1 ½ -gauge needle. The single cell suspension was then passed through a 70 µm filter. To concentrate the cells, the sample was spun down at 1,600 rpm for 8 min at 4°C. After decanting the supernatant, cells were re-suspended in ~300 µl of HBSS+ media and sorted in a BD FACSAria II.

To prevent rod contamination in the cone sort, rods were first sorted and a “rod gate” was created based on cell size (FSC) and granularity (SSC). During the cone sort, cells that fell in this rod gate were excluded.

FIXED sample preparation (RBC and CBC)

Dissociation was performed as mentioned above. Cells were then spun at 350 rcf at 4°C for 10 mins and resuspended in 250 uL of MEM, no glutamine with 4% Bovine Serum Albumin media (referred as MEM-B). Then 1 mL of Paxgene Tissue fix was added to the cell suspension and incubated at room temperature for 1 min. The sample was spun at 2,500 rcf for 2 mins and fixative was replaced with 1 mL of Paxgene Tissue stabilizer and incubated for 1 min at room temperature. Cells were spun again and stabilizer was replaced with 1 mL of PBS containing RNAsin Plus RNase inhibitor (1:100). Sample was washed one more time with the PBS containing RNAsin. Cells were then incubated with MEM-B containing 10% saponin and RNAsin (1:50) referred as MEM-BSR while gently shaking at 500 rpm for 5 mins at 4°C. Solution was then replaced with a 1:750 dilution of PKC antibody in MEM-BSR and cells were incubated for 30 mins while gently shaking at 4°C. After incubation, cells were rinsed twice with MEM-BSR. Solution was replaced with a 1:500 dilution of Goat anti-Mouse 647 antibody in MEM-BSR. Cells were incubated with secondary antibody for 30 mins while gently shaking at 4°C and then rinsed twice with MEM-BSR. Cells were concentrated in a final volume of 300 uL of MEM-B containing RNAsin (1:50) and sorted in a BD FACSAria II.

cDNA library construction

Cells were collected in Extraction buffer from the Arcturus PicoPure RNA Isolation kit after sorting and RNA was isolated using the same kit. mRNA was amplified in a linear fashion using the Arcuturus RiboAmp HS PLUS kit. cDNA libraries were generated using the TruSeq RNA Library Prep kit v2 and analyzed by 50 bp paired-end sequencing on an Illumina HiSeq 2000 platform.

RNA sequencing analysis

RNA sequencing reads were aligned to the reference mouse genome (GRCm38/mm10) using STAR (Dobin et al., 2013). Raw gene expression counts were calculated for annotated protein coding and lncRNA genes (Ensembl v. 86). Gene counts were generated for uniquely mapped reads using STAR. We excluded genes with low levels of expression. In total, 13,812 genes with expression level of CPM (counts-per-million) > 4 in at least one sample were kept for further analysis. Raw gene counts were then normalized using edgeR (TMM method, Robinson et al. 2010) and used for calculation of gene expression values as logCPM (log2-counts-per-million). Spearman correlation coefficients were calculated between each pair of samples using R (3.3.2)

Differential gene expression analysis

Differential gene expression analysis was performed using edgeR (Robinson et al. 2010) as described in (Chen et al. 2016). P-values were corrected for multiple tests using Benjamini-Hochberg false discovery rate (FDR) method implemented in R (3.3.2). We identified DE genes at FDR 5% with a minimum fold change cut-off greater than 4 (log2-fold-change or logFC > 2).

Annotation of cell surface and secreted proteins

We selected DE genes with an annotated signal peptide and/or one or more transmembrane domains. We then manually excluded known intracellular membrane-bound proteins (e.g. Golgi proteins). In this way, we compiled a list of 794 DE genes encoding putative CSPs, including plasma membrane-bound and secreted molecules (Figure 3B). First, we calculated enrichment of cell surface proteins (CSPs) among the lists of differentially expressed genes using Gene Ontology (GO, Ashburner et al. 2000). We defined genes associated with the broad GO category “plasma membrane” (GO:0005886) and its offspring terms. We used Fisher's exact test to estimate the significance of enrichment of cell surface and secreted proteins (CSPs) among

differentially expressed (DE) genes compared to the background set of genes used in analysis (13812 genes). Next, we performed a manual curation of putative CSPs among all identified DE genes. We selected DE genes with an annotated signal peptide and/or one or more transmembrane domains. We then manually excluded known intracellular membrane-bound proteins (e.g. Golgi proteins).

Comparison with published sequencing data

We compared expression profiles of differentially expressed CSPs between RBCs and CBCs to published single cell profiling of different subtypes of bipolar cells (Shekhar et al. 2016). Tables with normalized single-cell expression profiles and cell type identities from (Shekhar et al. 2016) were downloaded from Single-Cell RNA-Seq Portal (https://portals.broadinstitute.org/single_cell/). For each analyzed gene we calculated the percentage of cells in each bipolar subtype with expression value more than 0.

We also compared results of our analysis with recently published RNA sequencing data from wild-type rods (Nrl WT) and Nrl knockout (Nrl KO) mice (Kim et al. 2016). Normalized transcript expression profiles were downloaded from RetSeq Database (https://retseq.nei.nih.gov/). Expression values (FPKM) for different isoforms of same genes were summed together, and mean gene expression values were calculated for each cell type (i.e. Nrl WT or Nrl KO) at P14. Next, we calculated log2-fold-change in gene expressions between Nrl WT and Nrl KO as $\log FC_{WT/Nrl\text{-}KO} = \log_2(FPKM_{WT}) - \log_2(FPKM_{Nrl\text{-}KO})$. Similarly, we calculated log2-fold-change in gene expression between Rods and Cones at P13 in our dataset as $\log FC_{Rods/Cones} = \log_2(CPM_{Rods}) - \log_2(CPM_{Cones})$. In particular, we focused on comparison of $\log FC_{Rods/Cones}$ to $\log FC_{WT/Nrl\text{-}KO}$ values for CSPs differentially expressed between rods and cones (see Figure S4 F).

Plasmid Construction

Plasmids

For single sgRNA/Cas9 expression we used either px458 (Ran et al., 2013) or px330 (Cong et al., 2013). px458 contains coding sequences for SpCas9 and GFP separated by the T2A peptide, and expressed under the control of the Cbh promoter. After electroporation, native fluorescence of GFP from px458 was only partially visible at P6, moderately visible at P14 and bright at P21. To assess phenotypes at early ages, we co-

electroporated px458 with pJS1, in which the mCherry coding sequence was expressed under the Ubiquitin promoter and visible as early as P2.

In px330, Cbh only drives Cas9 expression. For *in vivo* fluorescent co-labeling, we used either pJS1, in which mCherry was expressed under the Ubiquitin promoter, or pCAG-IRES-GFP, in which eGFP was expressed under the CAG promoter.

To knockdown NRL via RNAi, we inserted annealed oligonucleotides after the U6 promoter in pLL3.7 (Rubinson et al., 2003) digested with *HpaI* and *XhoI*. Oligonucleotides included an Nrl shRNA-encoding sequence designed by Cepko and colleagues (Matsuda and Cepko, 2004), labeled shRNA1, and a second sequence designed ourselves. Oligonucleotide sequences used, shRNA1: 5' - tGGTCCTGTCTCTATGGAAGttcaagagaCTTCCATAGAGACAGGACCttttttc – 3' ; and 5' - tcgagaaaaaaGGTCCTGTCTCTATGGAAGtctcttgaaCTTCCATAGAGACAGGACCa – 3'; shRNA2: 5' - tGGGCCTCTTGGCTACTATTttcaagagaAATAGTAGCCAAGAGGCCCttttttc – 3'; and 5' - tcgagaaaaaaGGGCCTCTTGGCTACTATTtctcttgaaAATAGTAGCCAAGAGGCCCa – 3'.

A dominant negative NRL coding sequence was designed based on truncated *Nrl* cDNA sequences analyzed by Swaroop and colleagues (Rehemtulla et al., 1996). The Nrl acidic region (amino acid residues 23-127) was excluded from cDNA amplification, while other domains (DNA binding domain) were kept. The following primers were used to amplify truncated NRL from the full cDNA: fwd: 5' - TTGAGTCTAACCCAGGGCCAGATATGGCTTTCCCTCCCAGTCCCTTGGCTATGGAA TATGTTAATGACTTTGATTTGATGAAGTTCGAA – 3'; rev: 5' fwd: 5' - TCTAGAGTCGCGGCCGCGATTCAGAGGAAGAGGTGTGTGTGGTCG – 3'. Truncated Nrl was subcloned after the T2A sequence in a plasmid bearing the CMV promoter and mKate2 followed by T2A. PCMV:mKate2 T2A was cut with NotI. The oligonucleotides above hold 25bp overhangs that allow recombination between the vector and oligonucleotides.

To spatially manipulate Cas9 expression, we used four promoters in px458. In the outer retina, we found that Cbh and Ubiquitin (Matsuda and Cepko, 2004) regulatory elements drive expression of fluorescent reporters in Rods, Bipolar Cells and Muller Glia. We used

a 2.3 kb fragment of the Rhodopsin promoter to drive Cas9 expression in rods (Matsuda and Cepko, 2004; 2007), and a 1082 bp fragment containing a tandem repeat of an mGluR6-SV40 promoter (4XGrm6-Sv40) from the pAAV-4xGRM6-CatCh-EGFP vector (gift from Botand Roska) to drive Cas9 expression in ON BCs (van Wyk et al., 2017). Promoters were cloned between the KpnI and AgeI restriction sites in px458. In all cases, native fluorescence from GFP was visible by P21.

To multiplex sgRNAs, we modified the multiplex CRISPR vector system developed by Yamamoto and colleagues (Sakuma et al., 2014). We subcloned a BsaI site-bearing multiplex cassette (from the "A2" vector provided in the multiplex vector kit) into the XbaI site in px458, 190 bp downstream of the U6 promoter, creating a destination site for a new $U6^{prom}$:sgRNA cassette. We sequentially cloned sgRNAs into px330S and our new px458, then performed the multiplex reaction as published. All clones were confirmed by sequencing. Thus our single multiplexed vector expressed two guide RNAs, Cas9 and GFP.

CRISPR design

We designed at least two 20bp guide RNAs (sgRNAs) per gene, targeting either exon one or a common exon among splice isoforms using an algorithm developed by Zhang and colleagues (Hsu et al., 2013). Only guides with high specificity scores (>70), and low numbers of off-target sites were selected. SgRNAs were designed as complementary single strand oligonucleotides bearing CAAAG (forward oligo) or AAAC…C (reverse oligo) overhangs. Each complementary pair was annealed with T4 polynucleotide kinase and T4 ligase buffer, and ligated into BbsI restriction digest sites 3' of the RNA polymerase III U6 promoter in the px458 plasmid (Ran et al., 2013). For complete list of oligonucleotide sequences used to design CRISPR/Cas9 vectors, see Table S6.

Electroporation

We electroporated retinas of neonatal pups (12-36 hours) *in vivo* using a protocol developed by Cepko and colleagues (Matsuda and Cepko, 2004; Wang et al., 2014). Briefly, sharp end glass micropipettes are backfilled with 8-10uL of DNA mixed with Fast Green Dye (0.2X) using microloading pipette tips. DNA is diluted to a final concentration of 1ug/uL with 0.2X Tris-EDTA. We injected DNA into the subretinal space using a Femtojet express microinjector at 330 hPa for 1-2 pulses at 3.5 seconds. Five current

pulses (80V, 50ms ON, 950ms OFF) were applied across the head using paddle electrodes.

Histology/Immunohistochemistry/Immunocytochemistry

Retinal tissue

Following enucleation, eyes were fixed in 4% paraformaldehyde for 45 minutes on ice. (For labeling with antibodies, mGluR6, Cacna1s, we found that fixation in 4% paraformaldehyde for 10 minutes at room temperature gave stronger signal.) Cryosections (20µm) were washed for 20 minutes with 1 X PBS, then permeabilized and blocked for 30 minutes in blocking solution containing 0.3% Triton X-100 and 3% Donkey Serum (or Goat Serum) in 1XPBS. Slides were then incubated with primary antibodies diluted in blocking solution overnight at 4°C in a humidified chamber. Primary antibodies were used at the following concentrations: anti-calbindin (1:2000), anti-S-opsin (1:500), anti-PSD-95 (1:400), anti-PKC (1:1000), anti-Secretagogin (1:2000), anti-Bassoon (1:600), anti-mGluR6 (1:1000), anti-GFP (1:2000), anti-Chx10 (1:500), anti-recoverin (1:4000), anti-RBPMS (1:50), CACNA1S (1:2000), Cone Arrestin (1:1000). After 3 washes of 5 minutes with 1XPBS, slides were incubated with Alexa Fluor secondary antibodies and when necessary treated with a nuclear counter-stain either TOPRO3 for 2 hours at room temperature or DAPI for 30 minutes at room temperature. Finally, slides were washed 3 times for 5 minutes each with 1XPBS and mounted in Fluoromount-G or VectaShield.

Retinal cultures on coverslips

Retinal cells on coverslips (see below) were fixed in 4% paraformaldehyde for 15 minutes, washed with 1XPBS and incubated in blocking buffer (see above) for 30 minutes at room temperature. Coverslips were incubated with primary antibodies overnight at 4C at the following concentrations: anti-rhodopsin 1:150 (EMD Millipore), anti-S-opsin 1:300 (Santa Cruz Biotechnology), anti-MAP2 1:1000 (Novocastra Laboratories), anti-TUJ1 1:500 (Neuromics), anti-Chx10 1:200 (Santa Cruz Biotechnology), anti-RBPMS 1:1000 (EMD Millipore), anti-Thy1 1:2000 (Abcam), anti glutamine synthetase 1:250 (Abcam), anti-AP2 1:100 (Abcam), anti-mCherry 1:1000 (Thermo Fisher), anti-Nr2e3 1:100 (a gift from Jeremy Nathans at Johns Hopkins), anti-recoverin 1:300 (EMD Millipore), anti-Ryk 1:150 (Abgent), and anti-Ryk 1:150 (a gift from Yimin Zou at UCSD). Stained coverslips were mounted in DAPI Fluoromount-G (SouthernBiotech).

Generation of mGluR6 antibody

The mGluR6 antibody was custom made through the Standard 70-day protocol from Thermo Fisher. Brielfy, two New Zealand White rabbits (Specific Pathogenic Free) were immunized with a peptide corresponding to the last 19 amino acids of rat mGluR6 as described in Morgans et al., 2006. The peptide sequence was conjugated with the immunogenic carrier keyhole limpet hemocyanin (KLH) and injected at 0.50mg. Booster injections were given every 14 days, and serum collection was performed on Day 56 from initial immunization. Immunoreactivity was determined by ELISA and the animal with the highest titer (200000ng/mL) was used in all experiments.

Photoreceptor cultures

Coverslip preparation

Flame-sterilized 12-mm round glass coverslips (Chemglass) were placed in sterile 24-well culture plates (Corning). Coverslips were then coated with a thin layer of Basement Membrane Extract using several steps. We first incubated the coverslips overnight in 1:4 poly-D-ornithine in ddH2O at 4C then rinsed once in ddH2O and air-dried for 5 minutes. Coverslips were then coated with 3 mg/mL Type 2 PathClear Cultrex BME (Trevigen) diluted in Dulbecco's Modified Eagle's Medium (DMEM; BioWhittaker Lonza). 100uL of BME suspension was applied to each coverslip using pre-chilled pipette tips and 5 mL tubes to avoid polymerization of BME. Coverslips were incubated at 37°C overnight. To generate thin gel-based layers, wells were incubated with ddH2O for 15 minutes at room temperature, then washed with 400uL DPBS immediately before seeding of retinal neurons. Coverslips were stored at 37°C with 400uL of culture medium (see below) until seeding.

Retinal dissociation

Retinas were dissected from P3 mice in Hank's Balanced Salt Solution (HBSS) (Ward's Science) on ice. Retinas were washed in Ca- Mg- free HBSS (Gibco) and incubated in papain solution (40 units papain suspension (Worthington), 300 units DNase I (Sigma), 10 mM HEPES in HBSS; 2.5 mL for 4 retinas) for 18 minutes at 37°C. Papain solution was removed and inactivated with 1 mL low-ovomucoid (LO) solution (1.5% BSA (Sigma) and 1.5% ovomucoid (Worthington)) in Eagle's minimal essential medium (MEM). Retinas were gently washed again with 1 mL LO, then 2X with 1% BSA in MEM (MEM-B). MEM-B was replaced with photoreceptor medium (PRM, see below) and retinal tissue was

triturated 6X with a P1000 pipette tip. Cultures were seeded at 80,000 cell/well in 400uL PRM for low density experiments, and 400,000 cells/well for high-density experiments.

Magnetic cell sorting

To purify photoreceptors from dissociated retinal cells we used magnetic cell sorting. 4-6 retinas were dissociated as above with one exception, AMES buffer replaced MEM in all solutions. Retinal cells were suspended in 300µL 1% BSA/AMES and incubated with 2 µL rat anti-CD73 (Koso et al., 2009) or rat anti-CD133 (Lakowski et al., 2011) per 10^7 cells for 15 minutes at room temperature. Cells were washed with 1% BSA/AMES, centrifuged then resuspended in fresh 1% BSA/AMES, then incubated in 20 uL goat anti-rat magnetic microbeads per 10^7 cells for 15 minutes at room temperature. CD73/133-positive cells were separated from unbound cells in a magnetic column, then eluted by deactivating the magnet. Cells were seeded at 80,000 cells/well. Photoreceptor enrichment was confirmed by increased proportions of cells labeled by rod-specific antibodies (NR2E3, Rhodopsin) and a cone-specific antibody (S-opsin) and a decrease in proportions of cell labeled by non-photoreceptor markers (Bipolars cells: Chx10; Ganglion cells: RBPMS, Thy1; Muller Glia: Glutamine Synthetase, Amacrine cells: AP-2) (data not shown).

Culture conditions

Retinal neurons were cultured in in PRM, containing 2% B27, 50ng/mL brain-derived neurotrophic factor and 1X penicillin-streptomycin (Sigma) in Neurobasal (Gibco). Cultures were grown at 37°C in 5% CO2. After 24 hours, 100µL of media was removed, and cultures were replenished with 300µL of fresh PRM.

To analyze rod responses to Wnt proteins, cultures were first incubated at 37°C for 24 hours to allow adherence. Recombinant WNT5A, WNT5B or WNT3A were diluted in 0.2% BSA/PBS and added dropwise. A range of concentrations were tested for WNT5A/5B (100ng/mL, 500ng/mL, 1000ng/mL) and WNT3A (100ng/mL, 200ng/mL, 500ng/mL); however, we did not observe significant differences in outgrowth. Therefore, we used 100ng/mL of WNT protein for all experiments unless otherwise noted. Control cultures received 0.2% BSA/PBS alone.

Image Analysis

Retinal cryosections

Images of retinal cryosections were acquired by either an Olympus FluoView FV1000 or a Zeiss LSM780 confocal microscope. Single confocal planes are shown for all figures unless noted as maximum projections. FIJI 'Z-project' tool was used to generate maximum projections. Adobe Photoshop was used to adjust the levels of brightness and contrast.

Retinal cultures

Cultured retinal cells were imaged by the Zeiss Axio Imager Z1 (ApoTome) widefield microscope. Images of *Ryk*^{CRISPR} cultured cells (Figure 7E, S7) were acquired by an Olympus FluoView FV1000. Micrographs were analyzed in FIJI (https://fiji.sc/).

QUANTIFICATION AND STATISTICAL ANALYSIS

Phenotyping

In our pilot screen, 8/30 of total observed CRISPR knockouts exhibited abnormal outer retinas (Table S6). At least two images were scored (and averaged when quantified) for each CRISPR-mutant retina. All 8 phenotypes were observed in at least two animals cumulatively between both CRISPRs of each pair. We describe these phenotypes in Figures 5, 6 and S5. In all bar graphs, error bars represent standard error.

Neurite Outgrowth

Neurites in photoreceptor cultures were identified by the co-labeling of Rhodopsin, MAP2/TUJ1, and when necessary, RYK and/or mCherry. Rhodopsin labeling itself was sufficient to measure neurite length. Neurites were delineated and measured in FIJI by tracing neurites from the initial neurite protrusion until the terminal. In photoreceptor enriched cultures, only those neurites that did not contact other cells were included for quantification. Unless otherwise noted, a Student's T-test was performed to determine significance.

Bipolar CRISPR quantification

Retinas were co-transfected with pCAG-IRES-GFP and either Prkca CRISPR or Scgn CRISPR. The “spot” feature in Imaris (http://bitplane.com) was used to count the number of GFP-positive cells within the region of interest, the inner nuclear layer. Spots needed to have a diameter of 7µm and an ellipsoid shape of 5.93µm to be considered a bipolar cell. Next, the “surface” feature was used in the GFP channel to create a mask of the Scgn or PKC staining within the GFP transfected cells. The spot feature was used again with

the same criteria as described above to count the number of cells in the masked Scgn-positive channel. Spots that co-localized in the GFP channel and the masked Scgn channel were counted as transfected cells that retained Scgn expression. The spot feature could not be used to count the number of PKC transfected cells as this staining does not label the entire cell, and the program fails to recognize it as a “spot”. The ratio of +GFP cells to either +PKC or +Scgn were plotted for the Control (no sgRNA) and Prkca CRISPR or Scgn CRISPR.

HC sprouting

An HC sprout was considered aberrant if it extended at least 5 µm apically (into the ONL) beyond the HC plexus. Sprouts were tallied per 20 µm (depth) x 200 µm (width) imaged stack.

Rod-cone distance

Distances were measured between each electroporated rod terminal and its closest cone terminal within a single optical plane (1 µm), then normalized to the average OPL width across the width of each image (~200 µm). Normalized distances were averaged among all animals mutagenized with either empty vector or each CRISPR.

Rod soma migation

Thicknesses of rod layers were measured in retinal cross sections. Rods were identified by their unique chromatin pattern as well as absence of labeling by the bipolar-marker, Chx10. Rods within the region bounded by the retinal pigment epithelium and OPL were denoted as ONL rods. Rods between the OPL and Chx10-expressing bipolar cells were denoted as INL rods. Thickness was measured by obtaining average Y-values across 300 µm-wide sections for the RPE, OPL and inner boundary of the INL rods.

DATA AND SOFTWARE AVAILABILITY

Raw and processed data files from RNA sequencing are available at NCBI GEO under the accession number GSE98838.

Supplementary Tables:

Table S1. Total number of reads and uniquely mapped reads for each RNAseq sample, Related to Figure 2.

Table S2. Normalized expression values for all expressed genes, Related to Figure 2.

Expression is shown as mean logCPM (log2-counts-per-million) of the two biological replicates for each cell type and time point. Column “is_deg” indicates if the gene was found to be differentially expressed in the pairwise comparison.

Table S3. Expression values of known cell-type markers, Related to Figure 2.

Values are shown as CPMs (Counts per Million). Second column indicates in which cell type the gene has been used as a cell-specific marker in (Roesch et al., 2008; Macosko et al., 2015; Kim et al., 2016; Shekhar et al., 2016). Enrichment values are indicated in bold. NA signifies expression was not detected.

Table S4. List of differentially expressed (DE) genes for each pairwise comparisons, Related to Figure 2.

DE genes were identified at FDR 5% with a minimum fold change cut-off > 4 (log2-fold-change or logFC > 2). Notation (i.e. R.P7_P13.up) is listed as “CellType.Timepoint1_Timepoint2.Direction” and refers to the genes that were enriched in rods at P13 compared to P7. For cell-type comparisons, notation (i.e. RB_CB.P13.RB) is listed as “CellType1_CellType2.Timepoint.Direction” and refers to genes that were enriched in rod bipolars compared to cone bipolars at P13. Cell types are denoted as rods (R), cones (C), bipolars (BP), rod bipolars (RB), and cone bipolars (CB). Expression values are the mean between the two biological replicates and are listed as logCPM. Fold change values are given as logFC with the corresponding adjusted p-values (padj). Last column (“is_csp”) indicates which were annotated as putative cell surface and secreted proteins (CSPs).

Table S5. Gene Ontology (GO) term analysis on differentially expressed genes, Related to Figure 2.

Contrast indicates pairwise comparison of Table S4. Direction is defined as those genes that are either upregulated/downregulated or cell-type enrichment (i.e. “r” for rods, “c” for cones, “CB” for cone bipolars, or “RB” for rod bipolars). A total of 1,489 out of 13,812 genes expressed were associated with GO-term “plasma membrane” (GO:0005886). The “deg_num” is the number of differentially expressed (DE) genes, and the “pm_num” is the number of DE genes associated with plasma membrane. The “pm_frac” indicates fraction of plasma membrane associated genes among total number of DE genes. Fisher’s exact test p-values are shown in last column.

Table S6. Summary of phenotypes of genes knocked out via CRISPR/Cas9, Related to Figure 4.

All genes analyzed with CRISPR/Cas9. General candidate genes = manually selected cell surface/secreted molecules. Wnt candidate genes = manually selected members of the Wnt family expressed in the outer retina. Previously described genes = genes where whole animals knockouts have been implicated in development or gene expression in the outer retina. Bipolar genes = Prkca and Scgn in CRISPR assay. *Scgn CRISPR1 was not included in quantification (Figure S4C) as this sgRNA failed to reduce Scgn protein expression.

KEY RESOURCES TABLE

REAGENT or RESOURCE	SOURCE	IDENTIFIER
Antibodies		
Mouse monoclonal anti-Bassoon	Enzo Life Sciences	CAT#VAM-PS003; RRID:AB_10618753
Rabbit polyclonal anti-Calbindin	Swant	CAT#CB38; RRID:AB_10000340
Rabbit polyclonal anti-Cone Arrestin	Millipore	CAT#AB15282; RRID:AB_1163387
Chicken polyclonal anti-GFP	Abcam	CAT#ab13970; RRID:AB_300798
Mouse monoclonal anti-PKC	Abcam	CAT#ab31; RRID:AB_303507
Mouse monoclonal anti-PSD95	ThermoFisher	CAT#MA1-046; RRID:AB_2092361
Mouse monoclonal anti-Rhodopsin	Abcam	CAT#ab98887; RRID:AB_10696805
Rabbit polyclonal anti-mGluR6	ThermoFisher	Generated in S.L.Z. lab
Rabbit polyclonal anti-Secretagogin	Biovendor R&D	Cat#RD181120100; RRID:AB_2034060
Goat polyclonal anti-S-opsin	Santa Cruz Biotechnology	CAT#SC14363; RRID:AB_2158332
Mouse monoclonal anti-Lim1/2	DSHB	CAT#4F2; RRID:AB_531784
Guinea Pig polyclonal anti-RBPMS	PhosphoSolutions	CAT#1832-RBPMS; RRID:AB_2492226
TO-PRO-3 Iodide	ThermoFisher	CAT#:T3605
DAPI	Sigma	CAT#D9542
Rabbit polyclonal anti-Ryk	Abgent	CAT#AP7677b; Lot#:SH21031E; AnimalID:RB1494
Rabbit polyclonal anti-Ryk	Gift from Yimin Zou lab	(Liu et al., 2005)
PNA Alexa Fluor 594 Conjugate	Life Technologies	CAT#L32459;
Mouse monoclonal anti-CACNA1S	Millipore	CAT#MAB427; RRID:2069582
Goat polyclonal anti-Chx10	Santa Cruz Biotechnology	Cat#SC21690; *discontinued*
Rabbit polyclonal anti-Recoverin	Millipore	CAT#AB5585; RRID:AB_2253622
Rat anti-CD73	BioLegend	CAT#127210; RRID:AB_11219400
Rat anti-CD133	ThermoFisher	CAT#12-1331-80; RRID:AB_465849
Donkey anti-Chicken Alexa Fluor 488	Jackson Immunoresearch	CAT#703-545-155; RRID:AB_2340375
Donkey anti-Mouse Alexa Fluor 488	Jackson Immunoresearch	CAT#715-545-150; RRID:AB_2340846
Donkey anti-Mouse Cy3	Jackson Immunoresearch	CAT#715-165-151; RRID:AB_2315777

Donkey anti-Mouse Alexa Fluor 647	Jackson Immunoresearch	CAT#715-605-151; RRID:AB_2340863
Donkey anti-Goat Cy3	Jackson Immunoresearch	CAT#705-165-147; RRID:AB_2307351
Donkey anti-Goat Alexa Fluor 647	Jackson Immunoresearch	CAT#705-605-147; RRID:AB_2340437
Donkey anti-Rabbit Alexa Fluor 488	Jackson Immunoresearch	CAT#711-545-152; RRID:AB_2313584
Donkey anti-Rabbit Cy3	Jackson Immunoresearch	CAT#711-165-152; RRID:AB_2307443
Donkey anti-Rabbit Alexa Fluor 647	Jackson Immunoresearch	CAT#711-605-152; RRID:AB_2492288
Goat anti-Chicken Alexa Fluor 488	Molecular Probes	CAT#A11039; RRID:AB_142924
Goat anti-Mouse Alexa Fluor 488	Molecular Probes	CAT#A11029; RRID:AB_138404
Goat anti-Mouse Alexa Fluor 568	Molecular Probes	CAT#A11031; RRID:AB_144696
Goat anti-Mouse Alexa Fluor 647	Molecular Probes	CAT#A21236; RRID:AB_141725
Goat anti-Rabbit Alexa Fluor 568	Molecular Probes	CAT#A11011; RRID:AB_143157
Goat anti-Rabbit Alexa Fluor 647	Molecular Probes	CAT#A21244; RRID:AB_141663
Rabbit anti-beta tubulin III (Tuj1)	Abcam	CAT#AB18207; RRID:AB_444319
Rabbit polyclonal anti-Map2	Abcam	CAT#AB32454; RRID:776174
Rabbit polyclonal anti-mCherry		Generated in J.R.S. lab
Rabbit anti-Reep6	Gift from Anand Swaroop lab	(Veleri et al., 2017)
Rabbit polyclonal anti-dsRed	Clontech	CAT#632496; RRID:AB_10013483
Bacterial and Virus Strains		
DH5α Competent Cells	ThermoFisher	CAT#:18258012
Biological Samples		
Chemicals, Peptides, and Recombinant Proteins		
HBSS, calcium, magnesium	ThermoFisher	CAT#24020117
HBSS, no calcium, no magnesium	ThermoFisher	CAT#14170112
Papain	Worthington	CAT#LK003178
Fetal Bovine Serum	Sigma	CAT#F0926

Liberase	Sigma	CAT#05401119001
Paxgene	Qiagen	CAT#765112
Bovine Serum Albumin	Gemini Bio-Products	CAT#700-106P
MEM, no glutamine	Gibco	CAT#11090081
DNase I	Sigma	CAT# 10104159001
RNAsin Plus RNase Inhibitor	Promega	CAT#N2615
Saponin	Sigma	CAT#47036
10XPBS	VWR	CAT#101175-842
Triton-X100	Sigma	CAT#T9284
Normal Donkey Serum	Jackson ImmunoResearch	CAT#017-000-121
Normal Goat Serum	Invitrogen	CAT#G9023
1XTris-EDTA	Fisher Scientific	CAT#24731
FastGreen Dye	Sigma	CAT#F7252-5G
Penicillin-Streptomycin	Sigma	CAT#P4333
Neurobasal	ThermoFisher	CAT#21103049
BDNF	Peprotech	CAT#450-02
Critical Commercial Assays		
Arcturus PicoPure RNA Isolation kit	ThermoFisher	CAT#KIT0204
Arcturus RiboAmp HS PLUS kit	ThermoFisher	CAT#KIT0525
TruSeq RNA Library Prep kit v2	Illumina	CAT#RS-122-2001
RNeasy Mini kit	Qiagen	CAT#74104
Deposited Data		
Raw data files from RNA sequencing	NCBI Gene Expression Omnibus	GSE98838
Experimental Models: Cell Lines		
Experimental Models: Organisms/Strains		
Mouse: Rhoicre:(B6;SJL-Pde6b+ Tg(Rho-icre)1Ck/Boc)	Gift from XianJie Yang (Li et al., 2005)	RRID:IMSR_JAX:015850
Mouse: HRGPcre:(OPN1LW-cre)#Yzl)	Gift from XianJie Yang (Le et al., 2004)	
Mouse: Ai9:(B6.Cg-Gt(ROSA)26Sor$^{tm9(CAG-tdTomato)Hze}$/J)	Jackson Laboratories	RRID:IMSR_JAX:007909
Mouse: Ai14:(B6.Cg-Gt(ROSA)26Sor$^{tm14(CAG-tdTomato)Hze}$/J)	Jackson Laboratories	RRID:IMSR_JAX:007914

Mouse: Grm6:GFP((Grm6-EGFP)5Var)	Gift from Rachel Wong (Morgan et al., 2006)	
Mouse: Hb9:GFP:(B6.Cg-Tg(Hlxb9-GFP)1Tmj/J)	Jackson Laboratories	RRID:IMSR_JAX:005029
Mouse: $Ryk^{flox/flox}$	Gift from Yimin Zou (Hollis et al., 2016)	
Mouse: Dvl1 +/-, Dvl1 -/-	Gift from Anthony Wynshaw-Boris (Lijam et a., 1997)	
Oligonucleotides		
See Table S6		
Recombinant DNA		
PX330	Gift from Feng Zhang (Cong et al., 2013)	Addgene plasmid #42230
PX458	Gift from Feng Zhang (Ran et al., 2013)	Addgene plasmid #48138
Multiplex CRISPRs	Gift from Takashi Yamamoto (Sakuma et al., 2014)	Addgene Kit #1000000055
Rhodopsin promoter	Gift from Connie Cepko (Matsuda and Cepko, 2004)	(Addgene plasmid # 11156)
pAAV-4xGRM6-CatCh-EGFP	Gift from Botond Roska (van Wyk et al., 2017)	
pCAG-IRES-GFP (pCAGIG)	Gift from Connie Cepko (Matsuda and Cepko, 2007)	Addgene plasmid #11159
pLL3.7	gift from Luk Parijs (Rubinson et al., 2003)	Addgene plasmid # 11795
CMV:mKate2 T2A	(Yamagata and Sanes, 2012)	
For list of CRISPR vectors, see Table S6		
Software and Algorithms		
Zen		
Imaris	http://bitplane.com	
FIJI	https://fiji.sc/	
STAR	(Dobin et al., 2013)	
edgeR	(Robinson et al., 2010)	
GO analysis	(Ashburner et al., 2000)	
Other		
BTX Harvard Apparatus Tweezertrodes	Fisher Scientific	CAT#BTX450166

BTX Gemini X2 Electroporation System	Fisher Scientific	CAT#BTX452007

Figure 1

Figure 1: OPL development

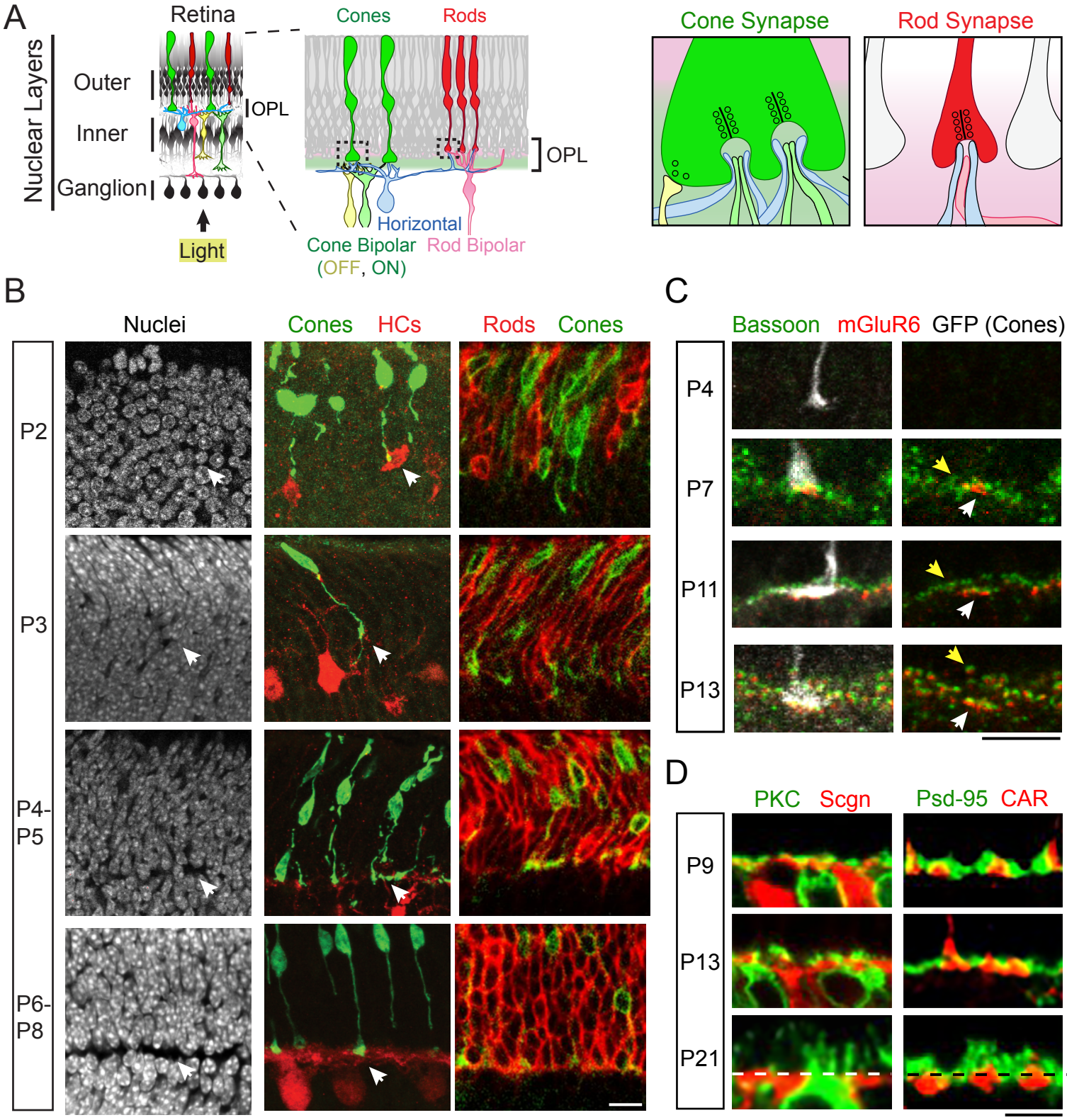
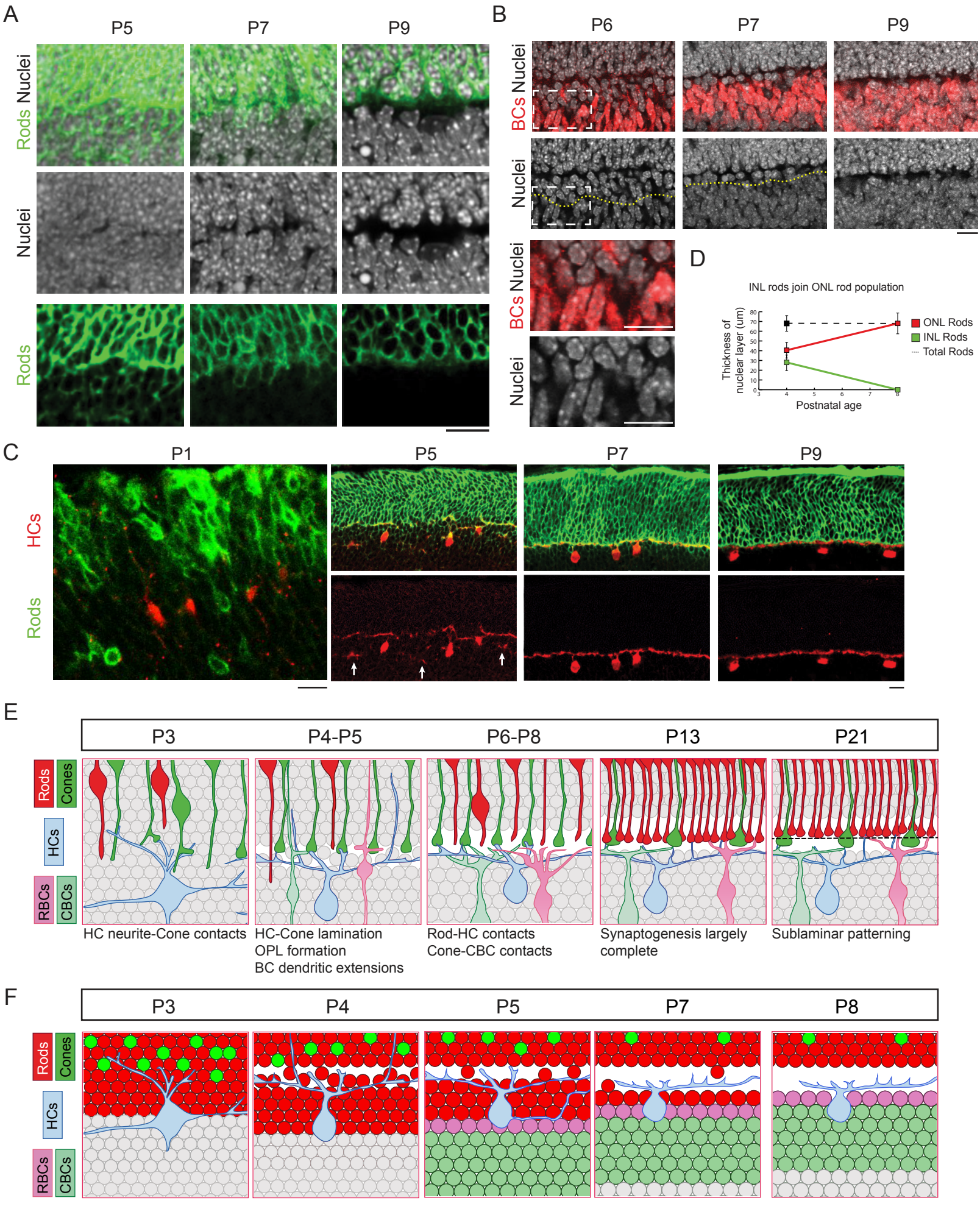


Figure 2. Rod migration and OPL development

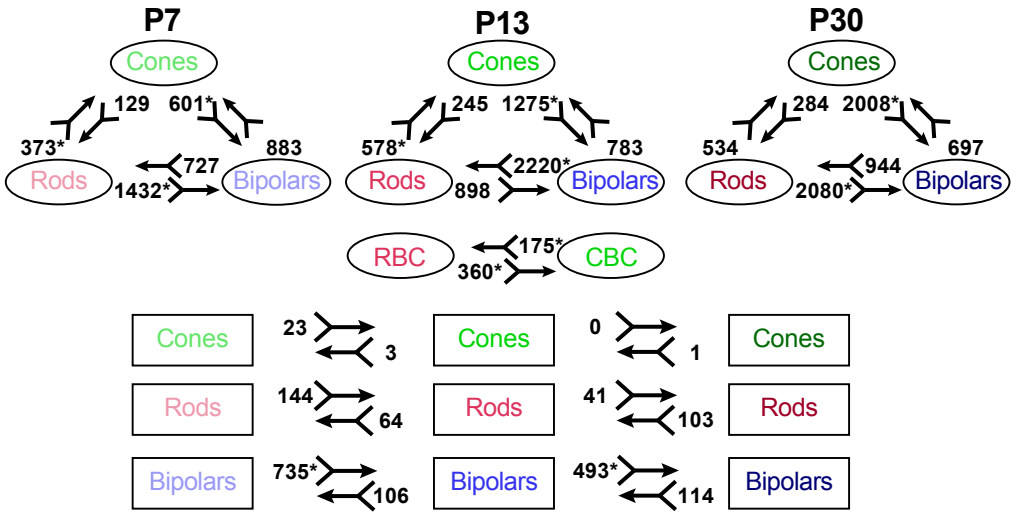


Figure

Figure 3: Bioinformatics

A

Summary of Differentially Expressed (DE) genes



B

Workflow for gene annotation

Differentially Expressed (DE) genes (2692)

↓

Annotated signal peptide and/or TM domain (1128)

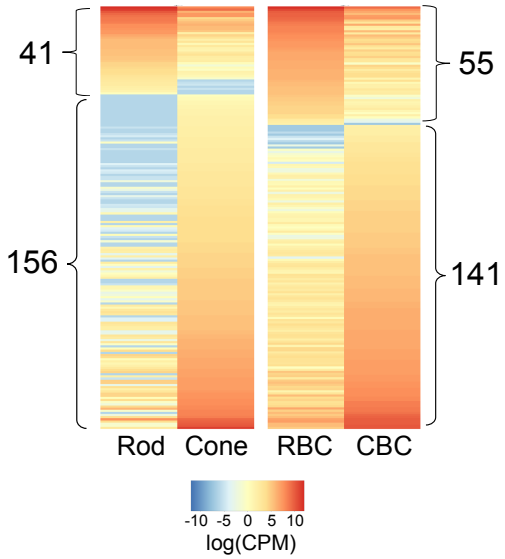
↙ ↘

Intracellular (335)

Cell surface (or secreted) (793)

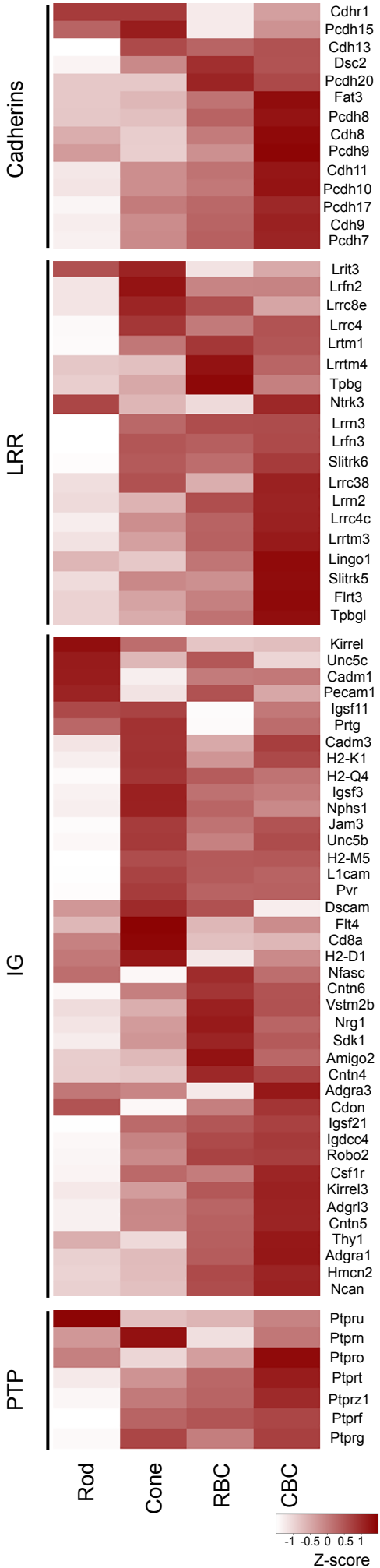
C

CSPs enriched at P13

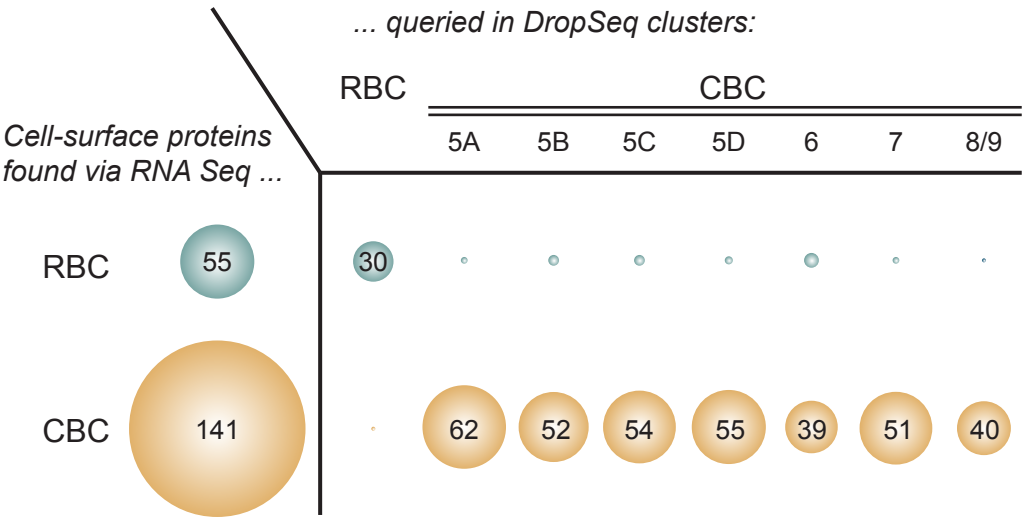


D

Unique cell-type enrichment of protein families

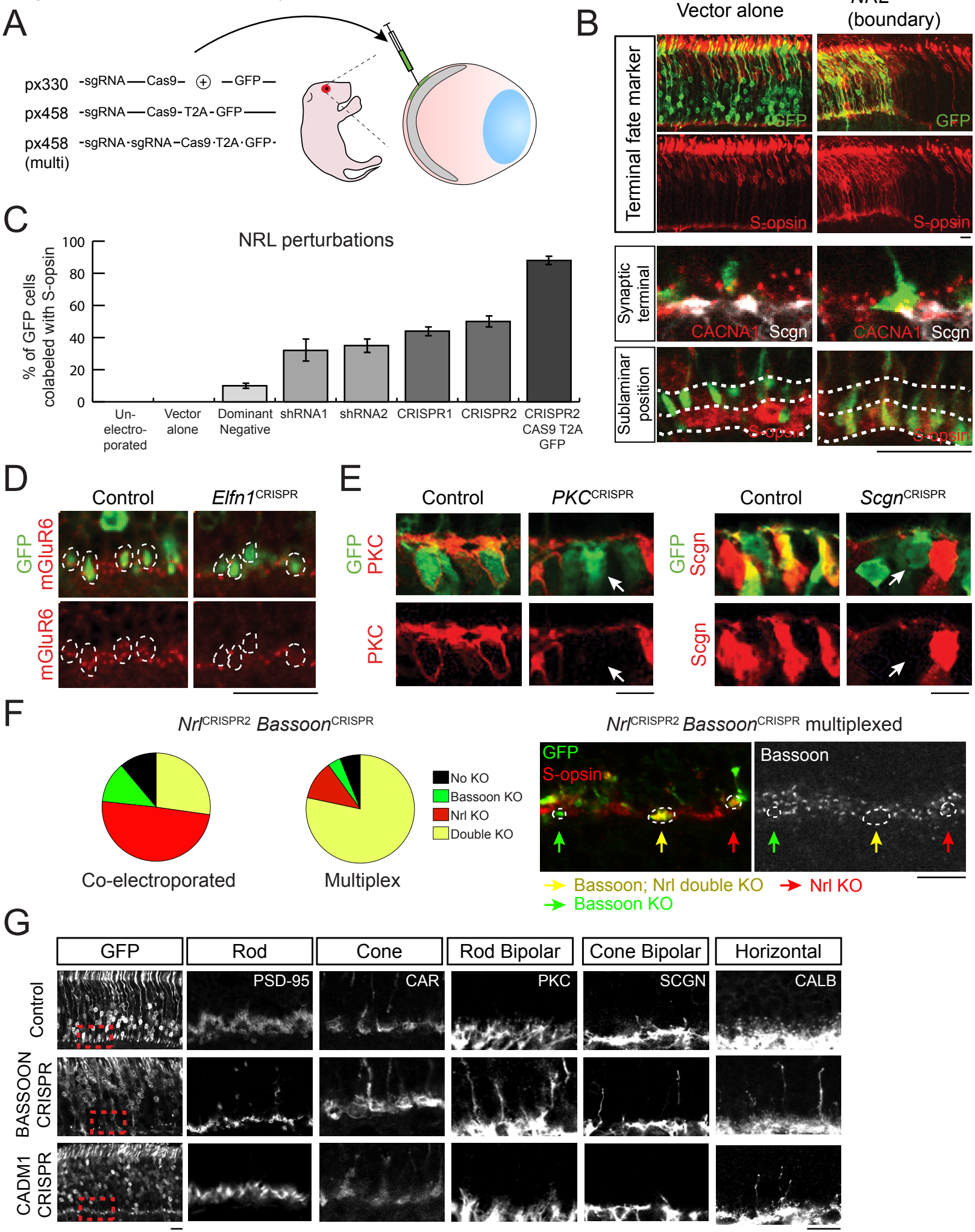


E



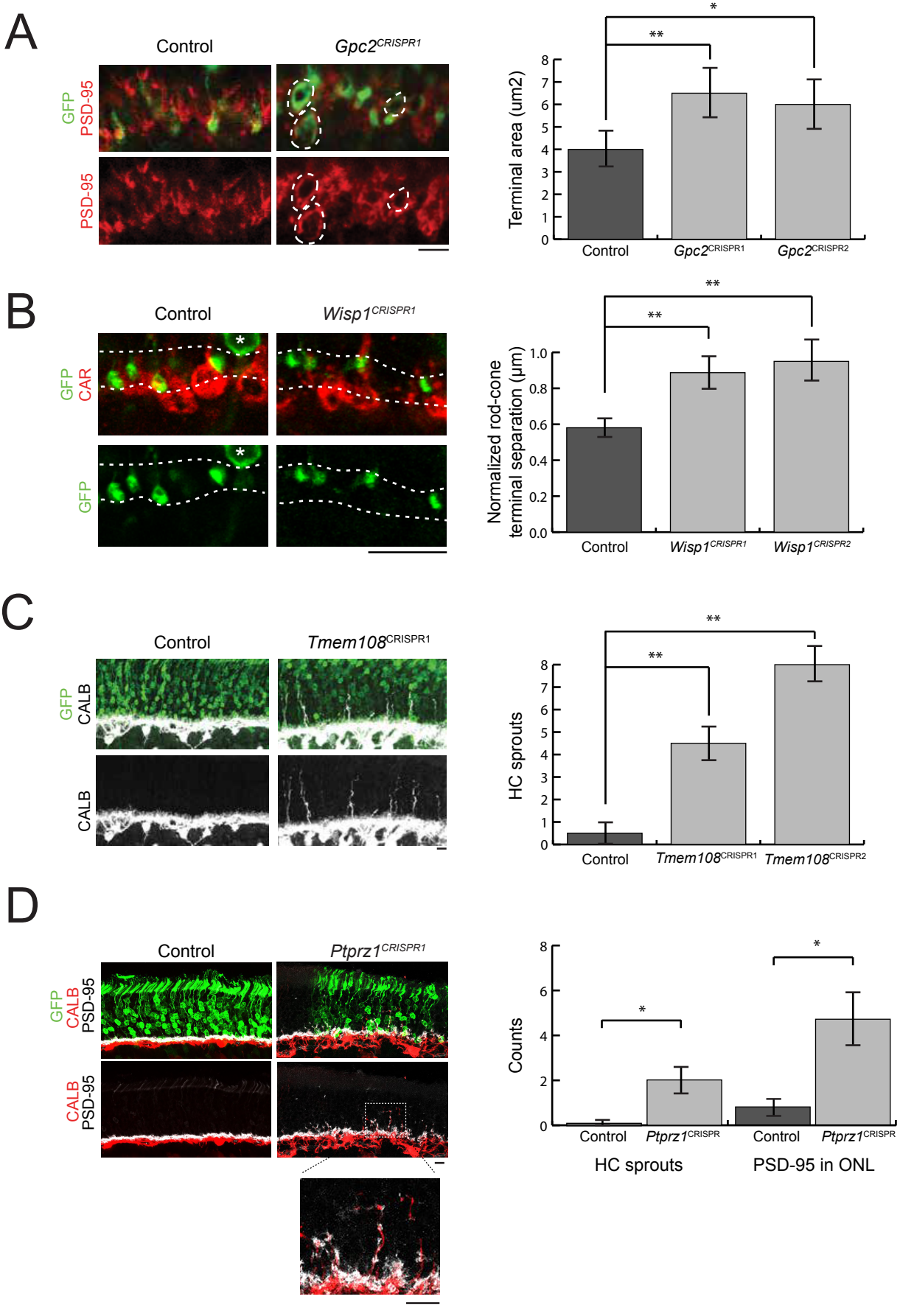
Figure

Figure 4: CRISPR assay



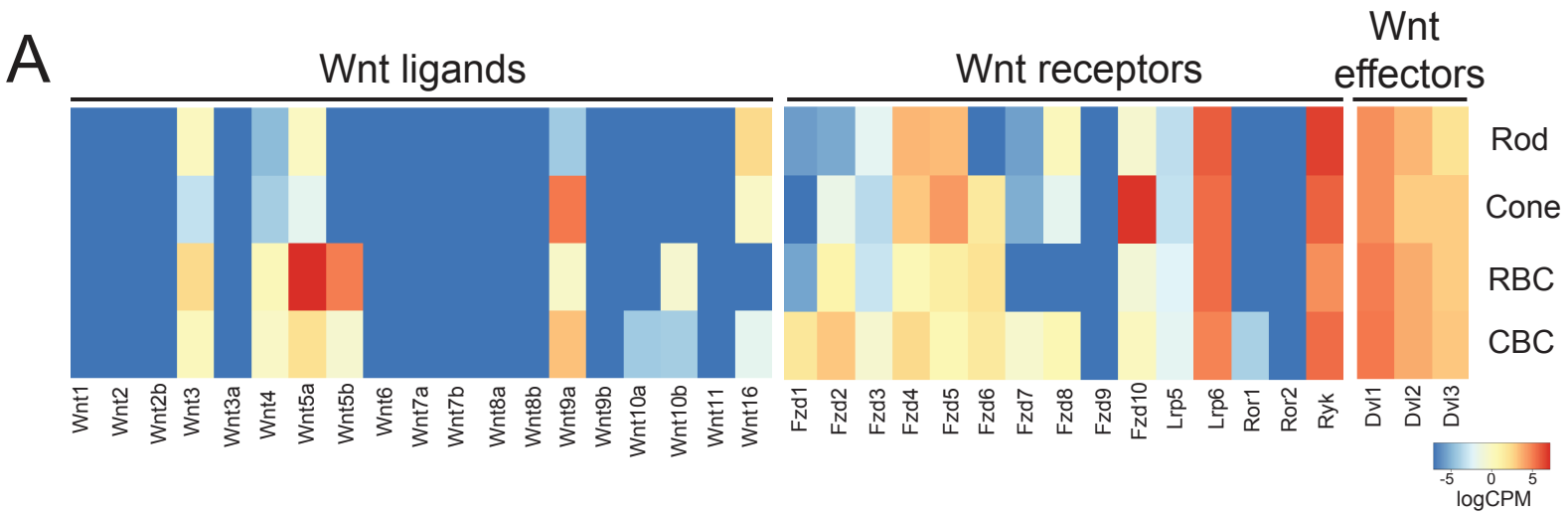
Figure

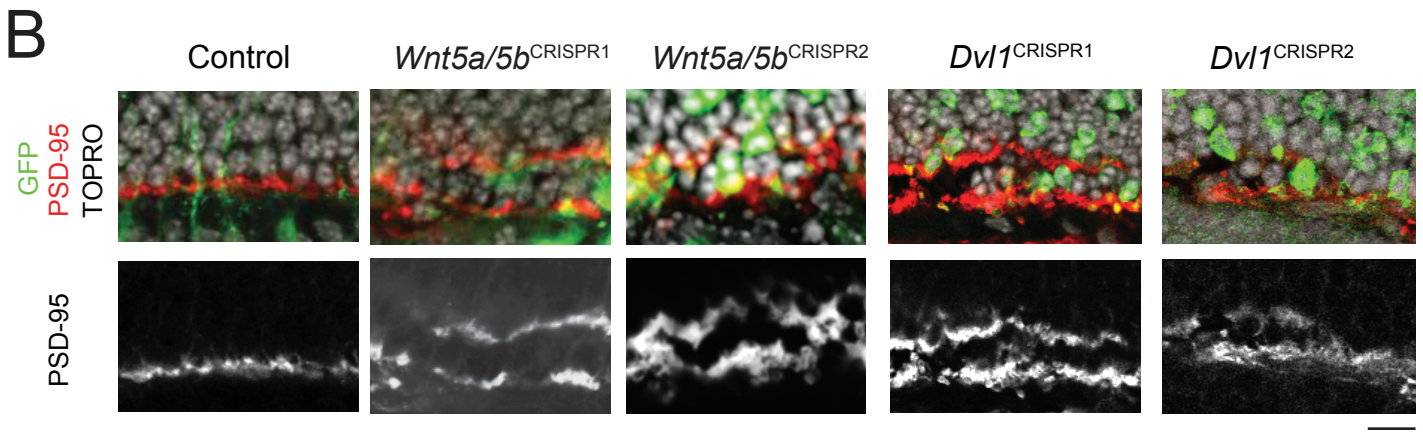
Figure 5: Phenotypes

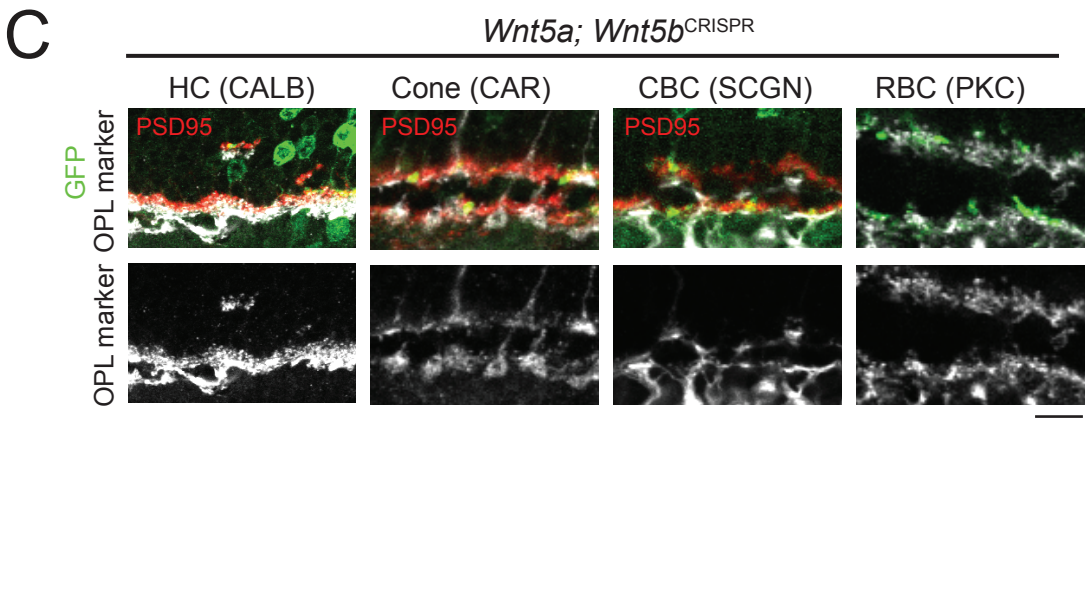


Figure

Figure 6. Wnts







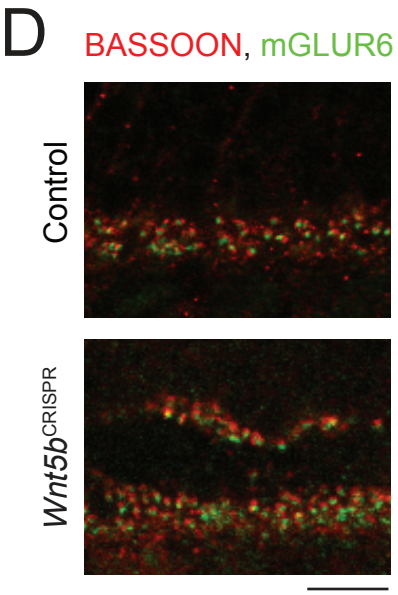
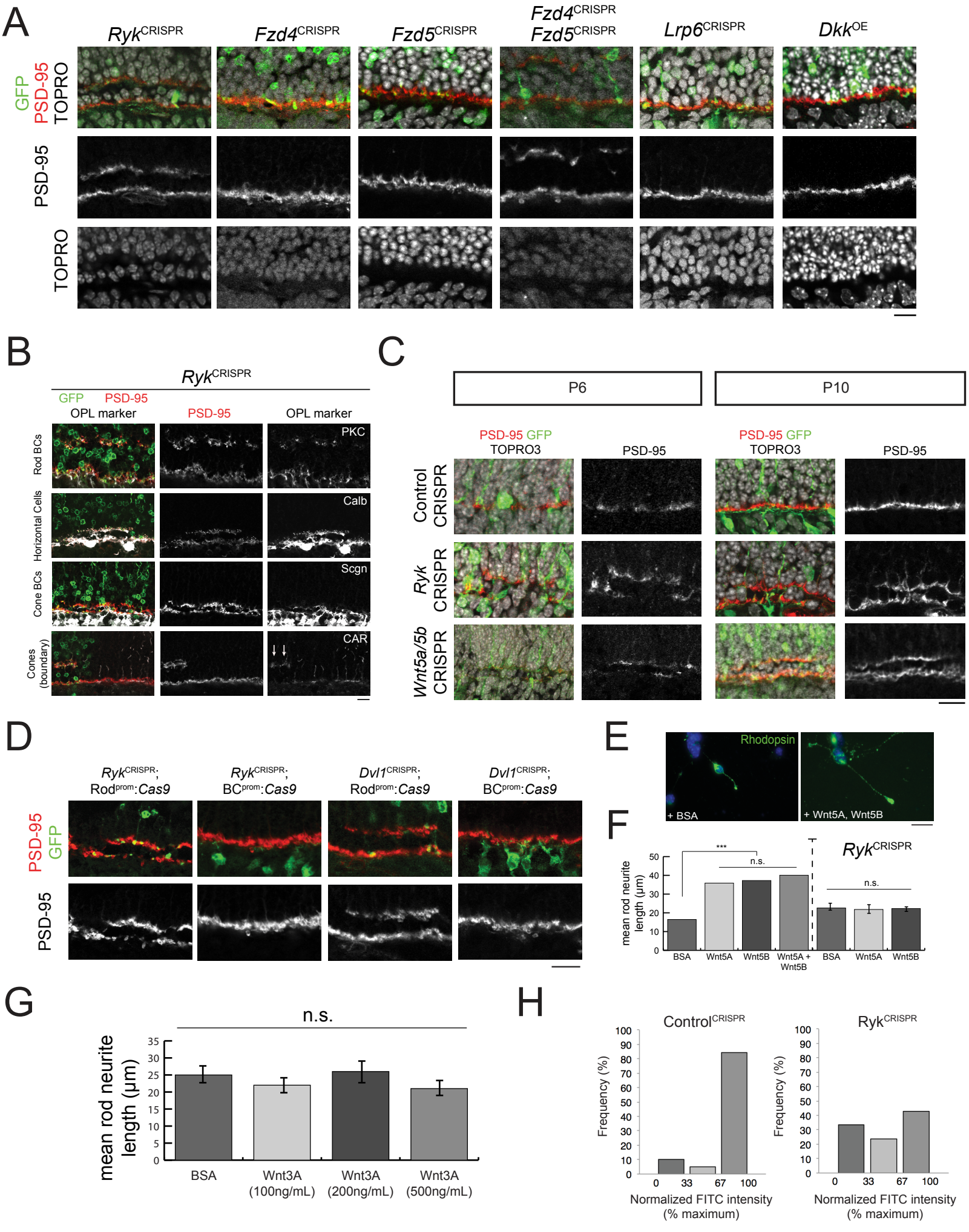


Figure 7. Testing a signaling pathway: Wnt5 acts through the Ryk-dependent pathway



Figure

Figure 8. Germline mutants and schematic

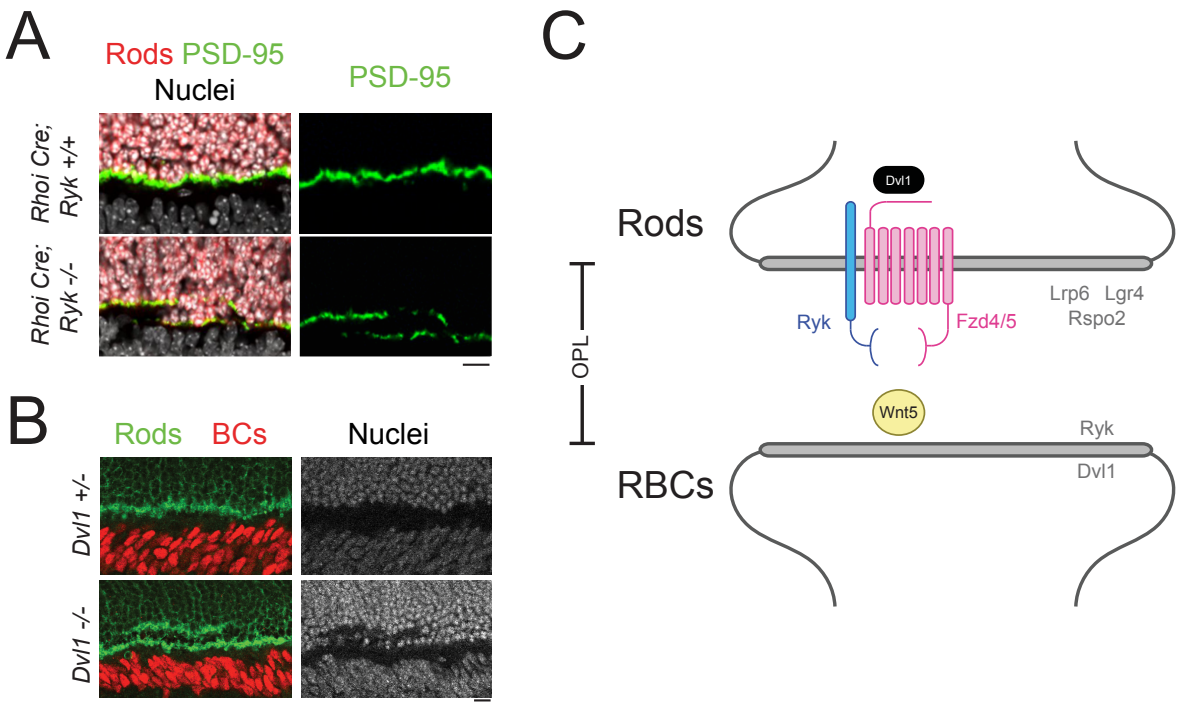


Figure S1, Related to Figure 1.

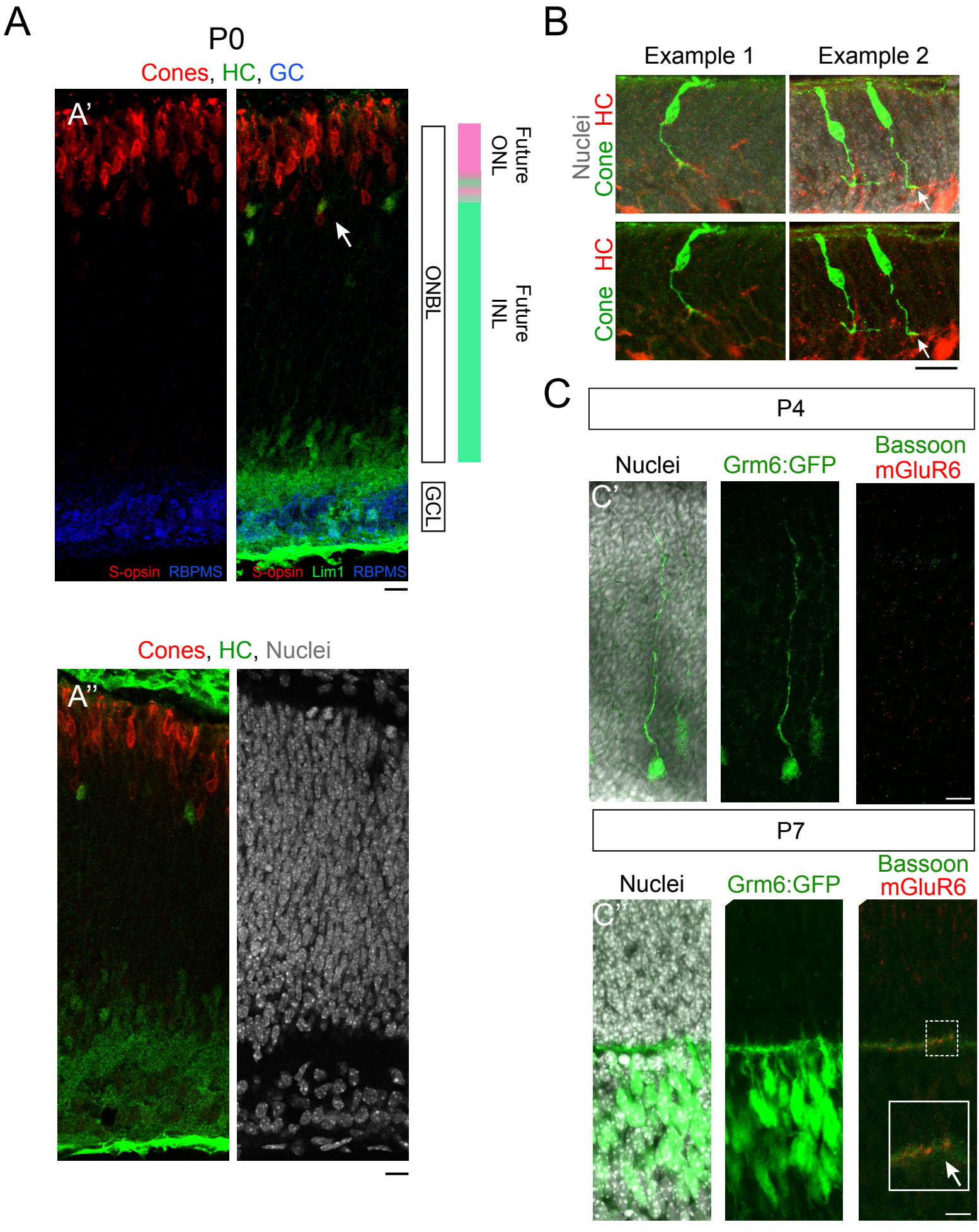


Figure S2, related to Figure 3

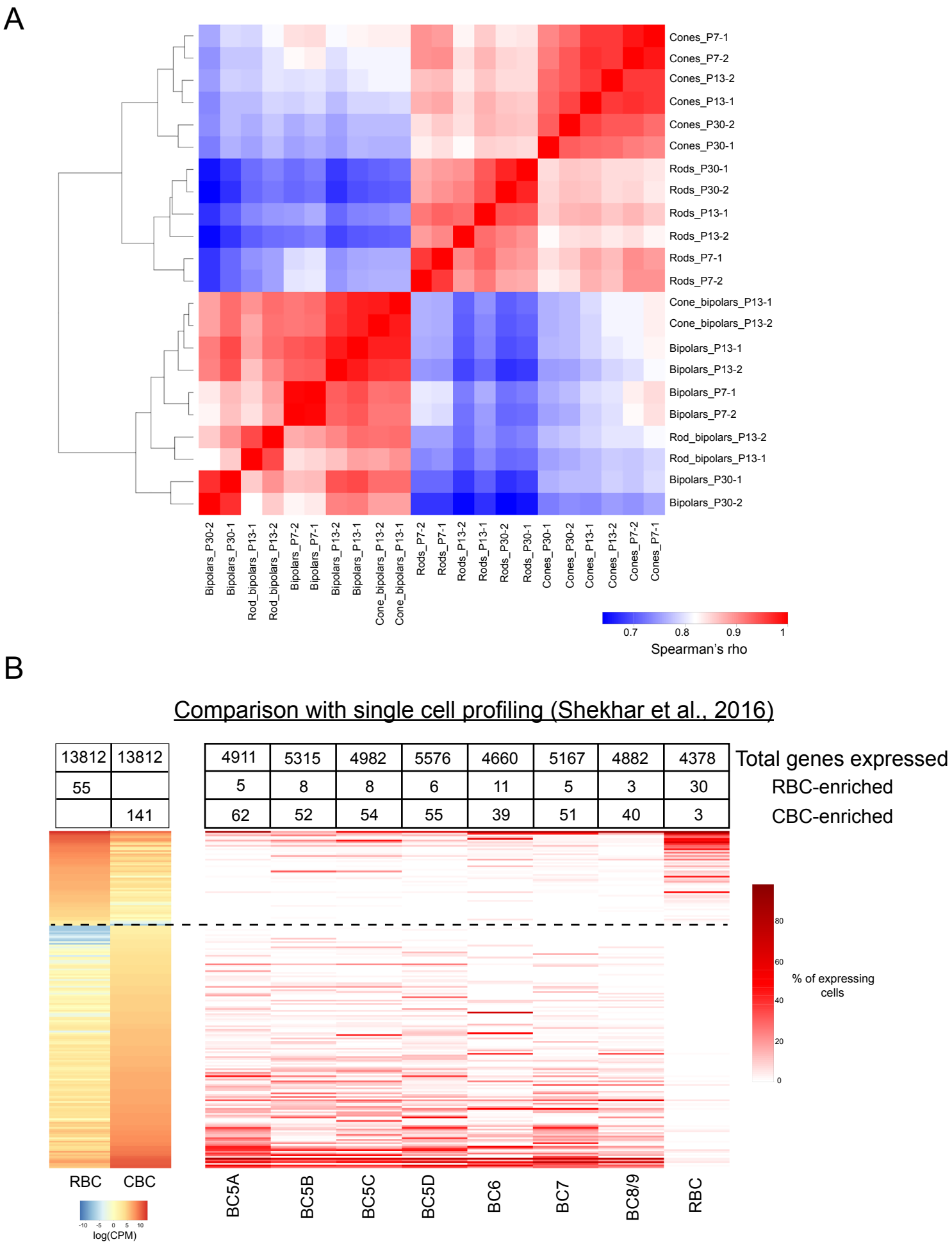


Figure S3. Related to Figure 3

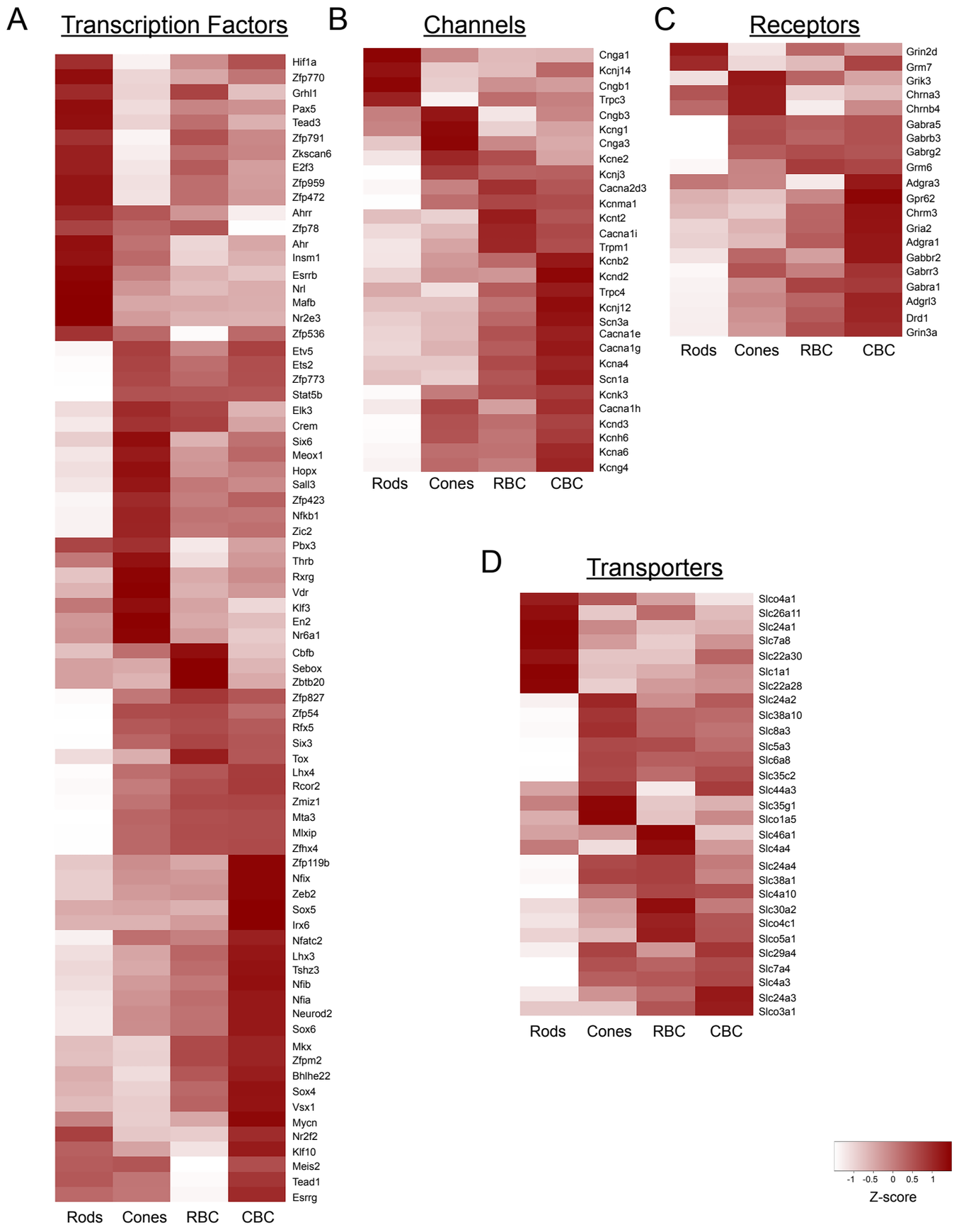


Figure S4. Related to Figure 4.

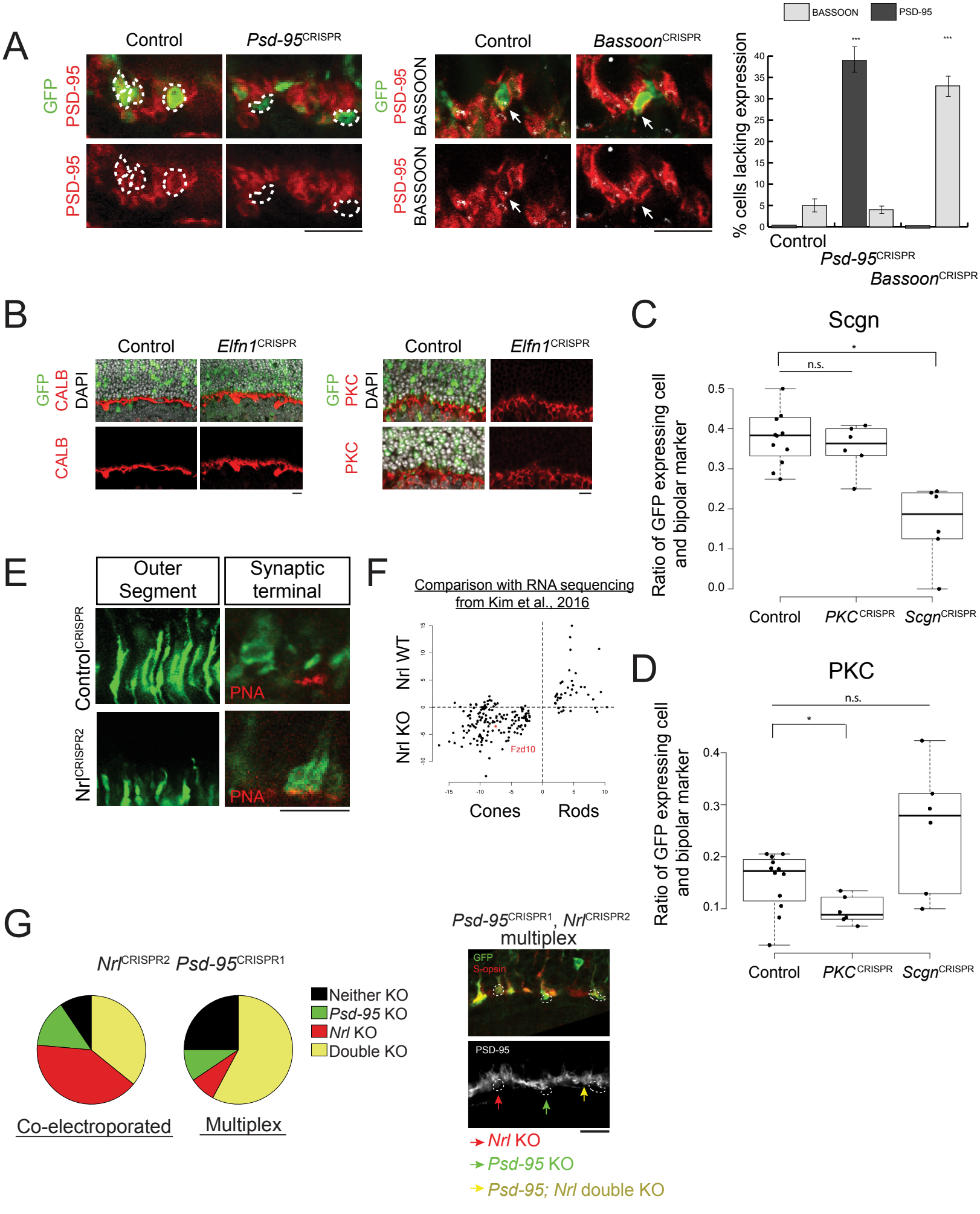
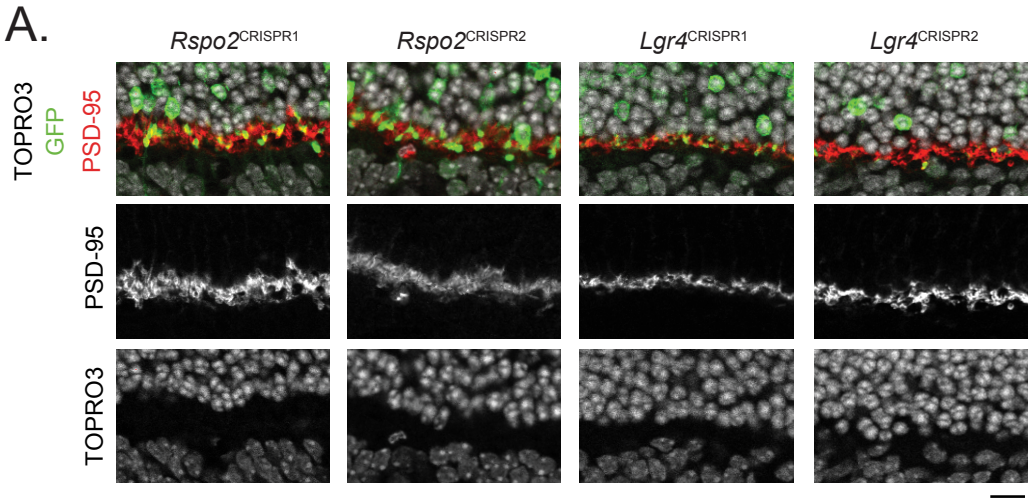
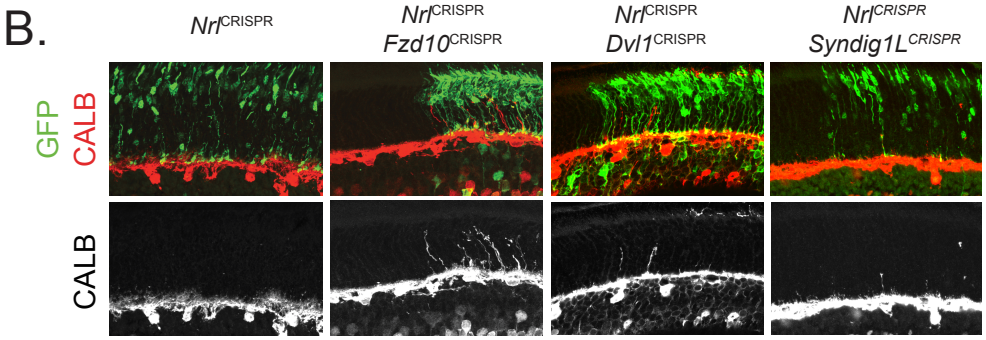
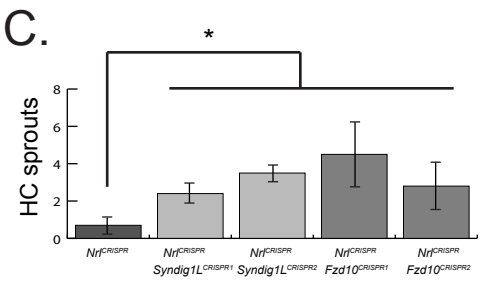
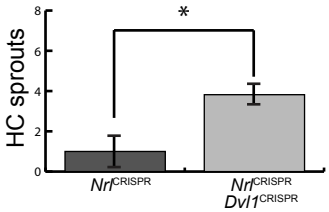


Figure S5. Related to Figures 5, 6









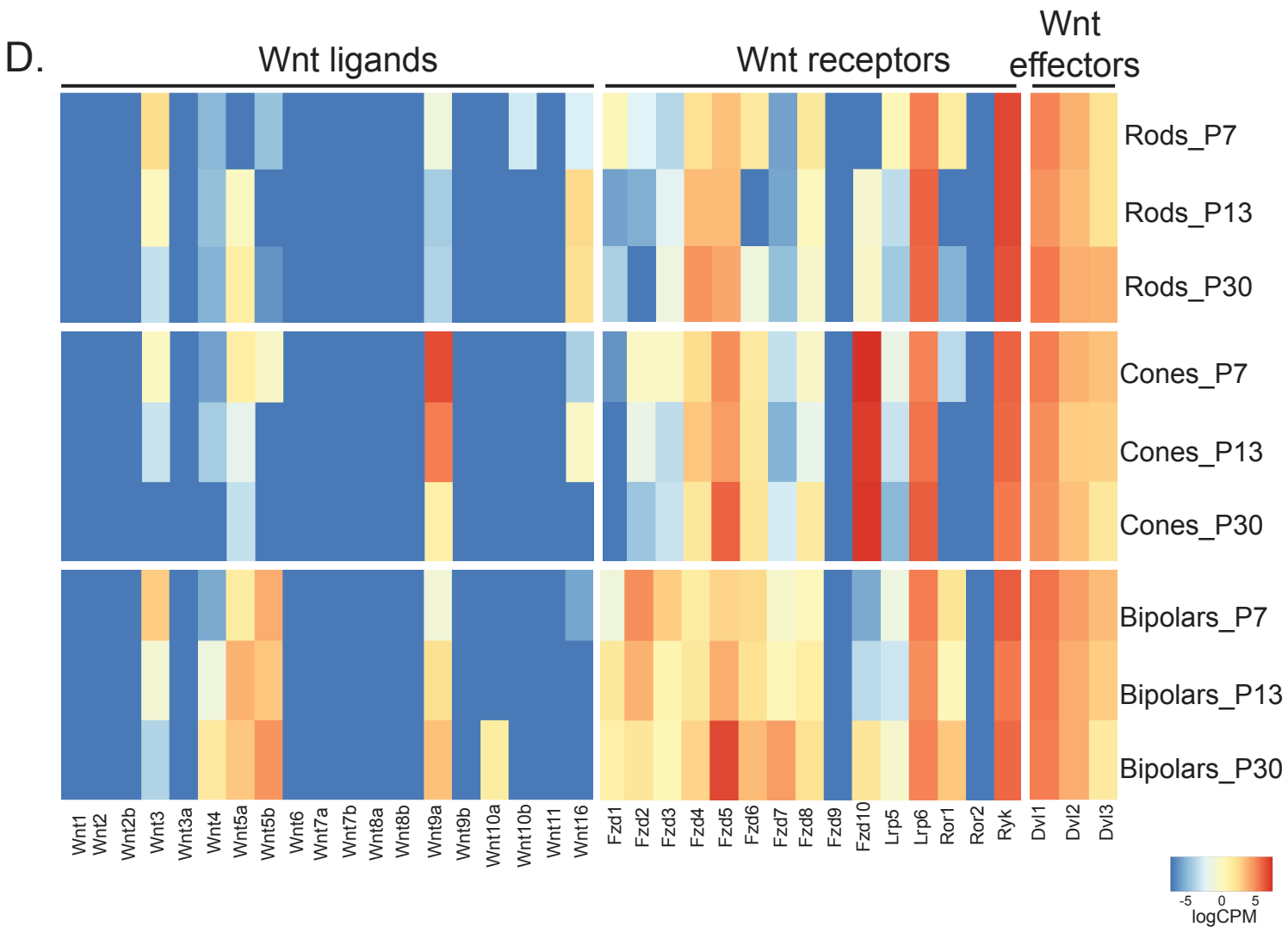


Figure S6. Related to Figures 5,6,7,8

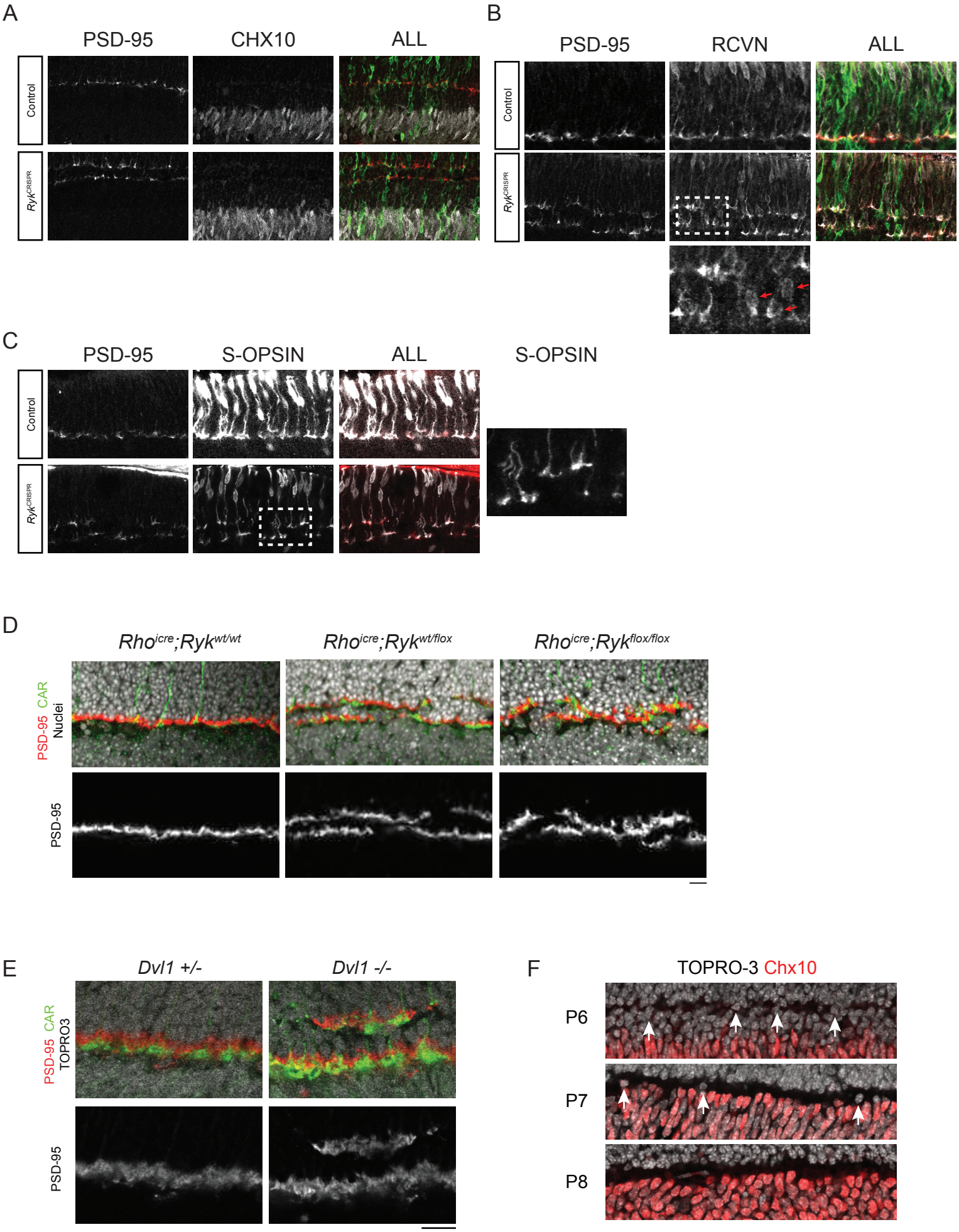
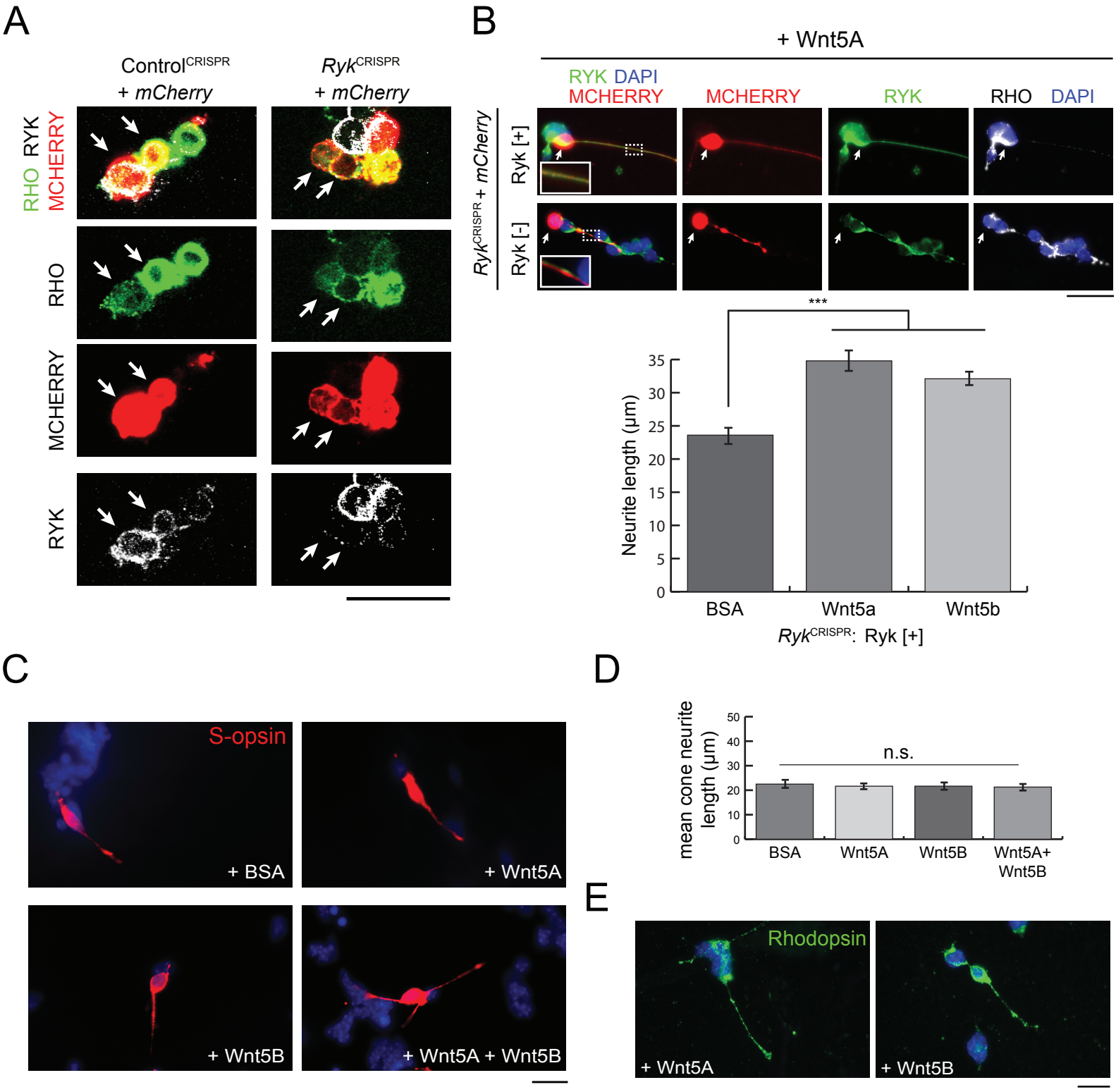
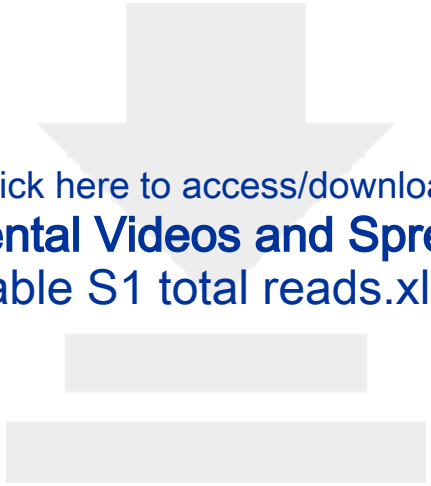


Figure S7. Related to Figure 6,7.





Click here to access/download

Supplemental Videos and Spreadsheets

Table S1 total reads.xlsx

Click here to access/download

Supplemental Videos and Spreadsheets

Table S2 all genes.xlsx



Click here to access/download

Supplemental Videos and Spreadsheets

Table S3 known markers v5.xlsx

Click here to access/download

Supplemental Videos and Spreadsheets

Table S4 DEGs v2.xlsx

Click here to access/download

Supplemental Videos and Spreadsheets

Table S5 GO terms.xlsx



Click here to access/download

Supplemental Videos and Spreadsheets

Table S6 - CRISPR phenotypes v6.xlsx